LITHOS 426–427 (2022) 106797

Contents lists available at ScienceDirect

LITHOS

journal homepage: www.elsevier.com/locate/lithos

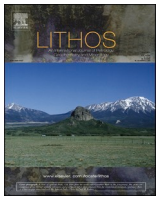

Age, geochemistry and mantle source of the Alto Diamantino basalts: Insights on NW Paraná Magmatic Province

Tommaso Giovanardi [a,*], Paulo Cesar Corrêa da Costa [b], Vicente A.V. Girardi [c], Ricardo K. Weska [b], Paulo M. Vasconcelos [d], David S. Thiede [d], Maurizio Mazzucchelli [a], Anna Cipriani [a,e]

[a] Dipartimento di Scienze Chimiche e Geologiche, Università di Modena e Reggio Emilia, Via Campi, 103, I-41125 Modena, Italy
[b] Faculdade de Geociências, Universidade Federal de Mato Grosso, Av. Fernando Corrêa da Costa, 2.367, CEP 78060-900 Boa Esperança, Cuiabá, Brazil
[c] Instituto de Geociências, Universidade de São Paulo, Rua do Lago, 562, Cidade Universitária, São Paulo 05508-900, Brazil
[d] School of Earth and Environmental Sciences, The University of Queensland, Brisbane, QLD 4071, Australia
[e] Lamont-Doherty Earth Observatory, Columbia University, Palisades, NY 10964, USA

ARTICLE INFO

Keywords:
Paraná basalts
Ar-Ar dating
Mantle source

ABSTRACT

The Paraná-Etendeka is one of the largest and most thoroughly investigated large igneous provinces in the world formed in a very narrow time-range (i.e., 1.6–3.0 Ma) between 135 and 132 Ma. The South American portion of this province, i.e. the Paraná Magmatic Province, is mainly characterized by a mafic magmatism of coeval low- and high-Ti magmatic terms. This bimodal activity has been explained by different degrees of melting of a homogenous mantle source or by plume activity and metasomatism of the sub-continental mantle. Despite the large body of literature, the true origin of the mantle source and processes leading to this bimodal magmatism are still debated.

In this work, we present the first geochronological, geochemical and isotopic data of basalts from Alto Diamantino (southern Mato Grosso, Brazil). These basalts have tholeiitic affinity and can also be classified in two different suites based on TiO_2 content (L-Ti < 3 wt%; H-Ti > 3 wt%) and Ti/Y (450 ppm), similarly to other volcanics from the Paraná Magmatic Province. Other geochemical parameters as Zr/Y and Nb/Yb ratios range from 3.78 to 8.60 and from 3.82 to 8.31, respectively. The L-Ti and H-Ti series have significant geochemical similarities, including $^{87}Sr/^{86}Sr$ ratios, with the Ribeira and Pitanga basalts of the Paraná Magmatic Province, respectively. The $^{40}Ar/^{39}Ar$ ages of the two series are statistically equivalent ranging between 134.4 ± 1.6 and 132.9 ± 2.0 Ma. Our data suggest that the Alto Diamantino basalts constitute the northwestern most expression of the Paraná Magmatic Province. Sr and Nd isotope ratios suggest that the original source of the Alto Diamantino basalts was a EM-I metasomatized mantle characterized by small amounts of different components (DMM and EM-II). Positive Ba and lack of Pb anomalies, together with K/Rb ratio, indicate the presence of amphibole in the mantle source of the Alto Diamantino basalts. Th/Nb and TiO_2/Yb ratios suggests that the compositional difference between the L-Ti and H-Ti basalts could be explained by different degree of melting at different depths of a heterogeneously metasomatized mantle source. The H-Ti group of basalts is compatible with low degrees of partial melting at depth while the L-Ti suite records larger degrees of melting. The metasomatic event occurred after the Mesoproterozoic, possibly during the Neoproterozoic formation of the Gondwana supercontinent.

1. Introduction

South America hosts several magmatic provinces related to the formation and break-up of supercontinents (Cordani et al., 2009; Giovanardi et al., 2019; Reis et al., 2021; Rocha-Júnior et al., 2020; Roverato et al., 2019; Teixeira et al., 2015, 2019). One of the most studied and largest magmatic provinces is the Paraná–Etendeka Magmatic Province (PEMP hereafter), which crops out in southeastern South America (Brazil, Argentina, Uruguay and Paraguay; Bellieni et al., 1984; Peate et al., 1990, 1992; Comin-Chiaramonti et al., 2013; Marques et al., 2016;

* Corresponding author.
E-mail address: giovanardi@unimore.it (T. Giovanardi).

https://doi.org/10.1016/j.lithos.2022.106797
Received 30 January 2022; Received in revised form 4 July 2022; Accepted 7 July 2022
Available online 12 July 2022

De Min et al., 2018; Machado et al., 2018; Gomes and Vasconcelos, 2021) and in southwestern Africa (Angola and Namibia; Ewart et al., 2004; Gibson et al., 2005; Comin-Chiaramonti et al., 2011). The PEMP is related to the Cretaceous break-up of the Gondwana supercontinent and the formation of the Southern Atlantic Ocean and was formed by a coeval bi-modal magmatism of high-Ti and low-Ti basalts with minor silicic lava flows and dykes. For several years, studies have been focused on the investigation of the mantle source, age, geodynamic setting and origin of PEMP leading to several different formation models largely discussed in literature.

Our study focuses on the first ever reported occurrence of basaltic lava flows outcropping in the Alto Diamantino region, at the northwestern border of the Paraná Basin. These basalts were described during the compilation of the geological map of the Mato Grosso state (Lacerda Filho et al., 2004), but without any further petrological investigation. Here, we provide the first comprehensive petrographic, geochronological and geochemical bulk data of these Alto Diamantino basalts.

The main goals of the present study are: 1) to determine the emplacement ages of the Alto Diamantino basaltic flows, 2) to chemically characterize and classify the basaltic lavas in the context of the high-Ti e low-Ti series previously identified in the Paraná Magmatic Province (PMP hereafter), 3) to constrain the origin and evolution of the parental mantle by using geochemical data and Sr-Nd isotopes and 4) to infer possible geotectonic implications.

2. Models for the PMP

In the past forty years, flood basalts from the PEMP have been intensively investigated. Our study is based on a new occurrence of basalts from the Alto Diamantino region situated in the South America continent, therefore we present first an overview of the current knowledge on the petrogenetic, geochronological and tectonic aspects of the PEMP, mainly focusing on magmatism in South America (Paraná Magmatic Province, PMP hereafter).

The Early Cretaceous volcanic rocks of the PMP were emplaced in the large intracratonic Paleozoic Paraná sedimentary basin, covering an area of 1,200,000 km^2 and containing 780,000 km^2 of extrusive rocks (Piccirillo and Melfi, 1988). Subalkaline (tholeiite) basalts are the dominant lithology with subordinate andesite, rhyodacite and rhyolite, the most silicic ones mainly being high-grade ignimbrites (Luchetti et al., 2018).

The first K-Ar geochronological determinations suggested that the main eruptive phase of the PMP basalts occurred at about 135–130 Ma (Rocha-Campos et al., 1988 and references therein). Whole-rock *Re*-Os dating yielded ages of 131.6 ± 2.3 Ma (Rocha-Júnior et al., 2012) and 130.9 ± 2.5 Ma (Correia et al., 2011). Baddelleyite/zircon U-Pb ages of felsic volcanic rocks yielded an age of 134.3 ± 0.8 Ma (Janasi et al., 2011). $^{40}Ar/^{39}Ar$ ages on plagioclase and whole-rock indicate 133–132 Ma as the more probable eruptive period, prior to South America and Africa separation (Renne et al., 1992). Thiede and Vasconcelos (2010) instead determined an $^{40}Ar/^{39}Ar$ age of 134.6 ± 0.6 Ma, suggesting that the extrusive process did not exceed 1.2 Ma. A recent re-evaluation of literature $^{40}Ar/^{39}Ar$ analyses with new K-decay constants and values for the Fish Canyon fluence monitor by Gomes and Vasconcelos (2021), returned Ar-Ar ages compatible with Thiede and Vasconcelos (2010). A review of all PEMP U-Pb and Ar-Ar ages constrains the timing of the magmatic peak between 135.0 ± 0.6 Ma and 132.0 ± 0.2 Ma with a time span of 1.6–3.0 Ma for duration of the extrusive process (Gomes and Vasconcelos, 2021).

In terms of chemical composition, the tholeiitic lava flows are representative of two different magmatic series: a high-TiO_2 (H-Ti) suite and a low-TiO_2 (L-Ti) suite, mainly outcropping in the Northern and the Southern PMP, respectively (Bellieni et al., 1984; Piccirillo et a al., 1989; Peate, 1997; Marques et al., 1999). The most accepted geochemical classification of the PMP basalts is the one proposed by Peate et al. (1992), who divides the two magmatic series in six compositional groups based on SiO_2, TiO_2, P_2O_5, Fe_2O_{3t}, Sr, Ba, Zr, Ti/Zr, Ti/Y, Sr/Y, Ba/Y and Zr/Y ratios. The groups are Gramado, Esmeralda and Ribeira for the low L-Ti suite and Paranapanema, Pitanga and Ubirici for the H-Ti suite.

Three main hypotheses have been proposed to explain the PMP origin and bi-modal composition. The first one attributes the genesis of the PMP basaltic lavas mainly to melts from the asthenospheric mantle produced by the passage of the South American plate over the Tristan da Cunha plume (Ewart et al., 1998; Gibson et al., 2005; Hoernle et al., 2015). A second hypothesis calls upon different degrees of partial melting of a common mantle source related either to the proximity of the Tristan da Cunha plume (Fodor, 1987) or to the influence of the lithospheric thickness on the extent of melting (Arndt et al., 1993). In any case, lower lithospheric levels and high pressures would limit the degree of melting favouring the production of H-Ti melts. Conversely, the production of L-Ti lavas, characterized by higher degree of melting and lower abundances of incompatible elements, would occur at shallower levels and lower pressures. Several studies advocate the role of the continental lithospheric mantle in the magma genesis at the PMP (Hawkesworth et al., 1988; Piccirillo et al., 1989; Marques et al., 1999) and at other Mesozoic flood basalts provinces, such as Karroo and Ferrar (e.g. Ellam and Cox, 1991; Mohlzahn et al., 1996).

Yet, difficulties in reconciling the geochemical and isotopic characteristics of the L-Ti and H-Ti suites with a homogeneous source require the involvement of a heterogeneous mantle source (e.g., Bellieni et al., 1984; Marques et al., 2016; Oliveira et al., 2018; Peate et al., 1992; Rocha-Júnior et al., 2013). This third hypothesis suggests that the two basaltic suites derived from a heterogeneous lithospheric mantle passively influenced by the thermal anomaly of the Tristan da Cunha plume (Peate et al., 1992). Further studies, focused on the Ubirici basalts, have brought into play the delamination of lithospheric mantle material and consequent mixing with the asthenosphere after continental break-up (Peate et al., 1999).

Combined geochemical and geophysical data suggest that regional thermal anomalies originated from the deep mantle rather than from a plume (Ernesto et al., 2002). According to this theory, a large thermal anomaly located in correspondence of the western African coast triggered the PMP basaltic magmatism. H-Ti tholeiites from the northern region of the Paraná Basin have been attributed to melting of a sublithospheric peridotite mantle veined or interlayered with mafic rocks, probably pyroxenites and eclogites, enriched with fluids or melts derived from slabs subducted during Neoproterozoic times (Rocha-Júnior et al., 2013). In this model the heat source is ascribed to a local combined effect of edge-driven convection and large-scale mantle warming under the Pangea supercontinent, while the contribution of the Tristan da Cunha plume is negligible. Review studies of the PEMP magmatism in Angola, Namibia and Eastern Paraguay (Comin-Chiaramonti et al., 2011, 2013 and references therein) and central PMP (De Min et al., 2018) identified the mantle source of the PMP with an anhydrous or phlogopite-bearing garnet peridotite veined by carbonatitic and/or alkaline melts. The enrichment of the lithospheric mantle is imputed to Proterozoic metasomatic melts with small-scale heterogeneity characterizing the H-Ti and L-Ti parental sources. Melting degrees of about 12 and 30% are suggested to produce the H-Ti and L-Ti respectively. Several studies (Comin-Chiaramonti et al., 2011, 2013; De Min et al., 2018; Ernesto et al., 2002; Rocha-Júnior et al., 2013) attributed the heat supply to regional thermal anomalies in the deep mantle without a large plume head intervention. Finally, it has been recently proposed that a heterogeneous mantle source containing Archean lithospheric fragments metasomatized by eclogite-derived melts during Neoproterozoic-Paleozoic is the source of northern L-Ti suite of the PMP magmatism (Rocha-Júnior et al., 2020).

The investigation of the tectonic aspects of the intrusive and extrusive tholeiites in Southern Brazil has led to the identification of a group of basaltic dykes, cropping out in the central-eastern region of the Rio Grande do Sul state, with a preferred NE-SW orientation and intruding

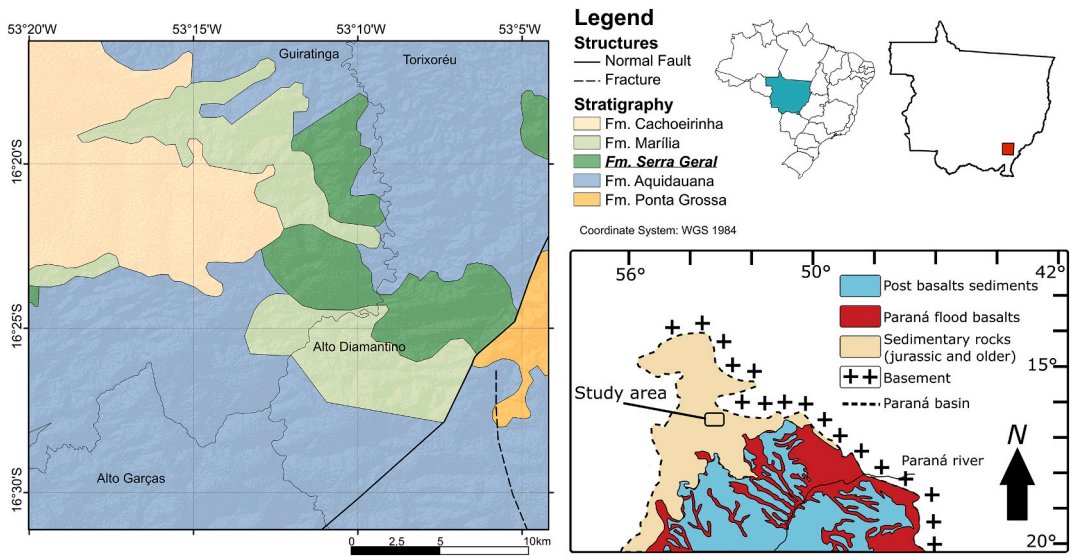

Fig. 1. Geological sketch map of the studied area and its position in the northern Paraná basin, modified from the regional map by Lacerda Filho et al. (2004).

the sedimentary rocks of the Paraná Basin (Sarmento et al., 2017). This direction coincides with the tectonic magmatic lineaments related to extensional processes and fault systems parallel to the Brazilian and Namibian coasts. This evidence suggests that the dikes are part of the triple junction system related to the opening of the South Atlantic Ocean. A second group of basaltic dykes intrudes flows of the Serra Geral Formation with a preferred NW-SE orientation, which suggests that they might be genetically related to the geotectonic cycles that originated the NW-SE oriented Ponta Grossa and Rio Grande Arcs and Torres Syncline.

3. Geological setting

The Alto Diamantino basalts are located in the northwestern PMP (Fig. 1). The area predominantly consists of Devonian to Tertiary sedimentary rocks (Fig. 1). Units description and their relationships is here integrated using notes of the geological map (Lacerda Filho et al., 2004).

The lowermost stratigraphic unit in the region is the Ponta Grossa Formation (Devonian), formed by ~50 m of laminated shales intercalated with subordinate arenites, often occurring in topographic lows. It is sometimes folded, more frequently at the top of the sequence. Upper and lower contacts could not be characterized, but non-conformable fault and erosional contacts with the overlying Aquidauana and Cachoeirinha units are reported in other Mato Grosso regions.

The Aquidauana Formation (Carboniferous), with 100 to 180 m thicknesses, dominates the landscape in the study area (Fig. 1). It contains conglomerates of quartz-arenites and silexite clasts in a quartz matrix cemented by iron oxide, overlain by white and red arenites. The arenites are generally medium grained and sometimes contain clay minerals or rare rock clasts. Laminated structures are common and cross bedding is present. The upper contact with the Cachoeirinha Formation (Neogene) is non-conformable erosive.

The Serra Geral Formation comprises mainly basalts outcropping in the central, southern and northeastern segments of the study area and includes the Alto Diamantino basalts (Fig. 1). The lavas are black, generally fresh, either represented by massive or columnar basalts. Weathered basalts can show spheroidal exfoliation and dark-green colour. Textures vary from aphanitic to fine-grained phaneritic and rarely amygdaloidal-vesicular textures are also present. Their estimated thickness varies from 100 to 150 m and the upper contact with the Cachoeirinha Formation is erosional. One outcrop in the south of the area consists of highly altered red basalts with 1 m thick veins of arenites, covered by altered conglomerate, breccia and argillite. This lithological association also occurs in the Salto das Nuvens Formation, defined in the Tangará da Serra region of Mato Grosso (Barros et al., 1982). This similarity suggests a possible stratigraphic correlation between the two formations. However, in the studied area these rocks constitute a local occurrence and the favoured idea is that these basalts belong to the Serra Geral Formation, whereas the sedimentary rocks to the upper sedimentary formations (Lacerda Filho et al., 2004).

The overlying Marilia Formation (Cretaceous) is formed by fine-grained arenites cemented by amorphous silica, lithic arenites and subordinate lenses of shales. The lithic arenites contain clasts of basalts and arenites cemented by calcite or dolomite. The lower contact with the Serra Geral Formation is non-conformable erosive, similar to the contact with the upper unit.

Conglomerates occur at the basis of the Cachoeirinha Formation (Neogene). These rocks contain gravels varying from cobbles to granules of quartz, iron oxide and arenites. The clasts are commonly cemented by iron oxide and rarely by silica cement. Red sandstones are at the top of the Cachoeirinha Formation. They consist of quartz with grain size varying from coarse grained to fine sand. The estimated thickness is up to 50 m.

Due to the fact that samples were collected in rare outcrops dispersed in the landscape (and not in boreholes), a stratigraphy of the lava flows was not recognized. However, L-Ti lavas mainly outcrop in the south-eastern part of Alto Diamantino, while H-Ti lavas occur in the north-western part (geographical coordinates of samples are reported in Supplementary Material 2).

4. Analytical methods

4.1. Ar-Ar dating

Three samples were dated by $^{40}Ar/^{39}Ar$ techniques on whole-rock at the UQ-Ages Laboratory of the University of Queensland, Australia. Fragments were crushed to <2 mm, washed in pure water in an ultrasonic bath, then washed for a minimum of 15 additional minutes first in distilled water and then in absolute ethanol and finally dried by compressed air. Ten to twenty grains 0.5 to 2 mm in size were hand-picked from the cleaned material under a binocular microscope. Up to five grains for each sample were loaded into a 21-pit Aluminium disk along with the neutron fluence monitor Fish Canyon Sanidine (age 28.201 ± 0.046 Ma; Kuiper et al., 2008), following the geometry illustrated in Vasconcelos et al. (2002). The irradiation disks were closed with aluminium covers, wrapped in aluminium foil, vacuum heat sealed into quartz vials, and irradiated for 14 h over the period from 25 January

Table 1
Major (wt%) and trace elements (ppm) of Alto Diamantino basalts.

Suite	L-Ti									
Sample	AD07	AD08	AD12	GBAS01	LL-03	LL-07	LL-08	LL-37	LL-70	T BAS-01
SiO_2	50.06	49.79	50.77	50.49	50.57	50.86	50.24	50.46	50.65	48.84
TiO_2	1.86	1.87	1.90	1.97	1.86	1.79	1.80	1.79	1.90	2.47
Al_2O_3	13.29	13.33	12.81	13.14	13.42	13.72	13.54	13.25	13.40	13.17
Fe_2O_3	1.60	1.60	1.68	1.68	1.68	1.59	1.57	1.59	1.63	1.70
FeO	11.86	11.87	12.47	12.44	12.42	11.77	11.61	11.81	12.08	11.94
MnO	0.21	0.16	0.21	0.20	0.21	0.24	0.16	0.27	0.22	0.23
MgO	6.40	6.94	6.45	5.90	6.07	5.89	7.00	6.62	5.87	6.27
CaO	9.88	9.66	10.07	9.80	10.07	10.16	9.50	10.30	9.99	8.77
Na_2O	2.27	2.16	2.26	2.33	2.34	2.36	2.23	2.21	2.37	2.19
K_2O	0.80	0.77	0.83	0.91	0.86	0.86	0.80	0.83	0.94	0.68
P_2O_5	0.20	0.19	0.21	0.22	0.21	0.21	0.20	0.20	0.22	0.26
LOI	0.42	0.80	0.18	0.38	0.40	0.44	1.12	0.50	0.48	1.16
Total	98.85	99.13	99.85	99.46	100.11	99.89	99.76	99.82	99.75	99.09
Mg#	0.51	0.51	0.51	0.52	0.50	0.54	0.51	0.53	0.49	0.48
Rb	14	14	16	17	18	19	17	17	22	5.7
Sr	255	253	261	266	267	285	295	271	290	260
Y	27	25	27	32	27	31	39	29	32	37
Zr	114	112	126	130	131	138	156	129	148	140
Nb	10	10	11	15	11	12	11	11	12	13
Cs	0.460	0.122	0.177	0.276	0.063	1.236	0.129	0.290	0.136	0.213
Ba	222	208	247	253	249	277	226	254	371	301
La	16	15	18	18	17	18	17	17	19	22
Ce	32	30	36	37	36	39	32	35	38	44
Pr	4.1	3.9	4.5	4.8	4.7	5.0	5.0	4.6	5.1	5.6
Nd	17	17	19	20	20	21	22	20	22	24
Sm	4.2	4.0	4.5	4.8	4.7	5.0	5.1	4.6	5.1	5.6
Eu	1.40	1.34	1.46	1.52	1.49	1.64	1.65	1.52	1.61	1.79
Gd	4.5	4.3	4.7	5.1	4.5	5.5	5.8	5.2	5.6	6.2
Tb	0.721	0.690	0.757	0.822	0.811	0.872	0.944	0.818	0.909	0.973
Dy	4.4	4.2	4.6	5.0	4.8	5.1	5.4	4.8	5.3	5.9
Ho	0.938	0.880	0.983	1.07	1.01	1.45	1.20	1.12	1.61	1.27
Er	2.5	2.3	2.6	2.9	2.9	3.1	3.2	3.0	3.4	3.4
Tm	0.373	0.345	0.387	0.426	0.432	0.450	0.464	0.438	0.498	0.491
Yb	2.33	2.14	2.45	2.66	2.64	2.85	2.79	2.74	3.1	3.1
Lu	0.345	0.318	0.358	0.394	0.407	0.437	0.433	0.425	0.495	0.449
Hf	2.95	2.86	3.3	3.4	3.5	3.6	3.4	3.3	3.8	3.7
Ta					0.941	0.744		0.689	0.794	
Pb	2.37	2.32	2.62	2.82	3.6	2.88	2.26	2.58	2.98	3.2
Th					2.00	2.02	1.86	1.91	2.15	
U	0.309	0.301	0.345	0.402	0.406	0.396	0.351	0.372	0.464	0.386

Suite	L-Ti							
Sample	T BAS-37	T BAS-38	WR-02B	WR-09	WR-16	WR-29	WR-32	WR-62
SiO_2	50.07	50.88	50.51	50.84	51.51	50.64	50.61	50.86
TiO_2	1.83	2.49	1.90	1.98	2.01	2.40	1.91	1.93
Al_2O_3	13.29	12.93	13.17	13.25	13.84	12.96	13.39	13.90
Fe_2O_3	1.66	1.74	1.65	1.69	1.58	1.80	1.65	1.57
FeO	11.06	11.49	12.25	12.54	11.68	13.36	12.20	11.60
MnO	0.21	0.33	0.21	0.22	0.20	0.21	0.22	0.26
MgO	6.53	5.01	6.06	5.52	5.20	4.68	5.92	5.31
CaO	9.80	9.08	9.98	9.95	9.41	9.25	9.93	9.66
Na_2O	2.24	2.40	2.37	2.41	2.47	2.15	2.37	2.54
K_2O	0.79	1.10	0.85	0.87	1.12	1.03	0.87	0.95
P_2O_5	0.20	0.31	0.21	0.22	0.24	0.29	0.22	0.23
LOI	0.98	0.34	1.04	0.51	0.65	0.99	0.28	0.58
Total	99.56	99.38	100.20	100.00	99.90	99.77	99.57	99.30
Mg#	0.51	0.52	0.48	0.48	0.51	0.47	0.44	0.45
Rb	12	20	18	18	27	39	19	20
Sr	250	250	308	281	290	277	287	303
Y	27	40	29	29	36	38	30	33
Zr	112	156	173	142	157	171	145	156
Nb	10	15	12	12	13	15	12	13
Cs	0.298	0.690	0.116	0.121	0.462	3.6	0.287	0.456
Ba	205	385	265	278	303	463	266	289
La	15	22	18	19	21	23	19	20
Ce	31	47	37	37	40	44	37	40
Pr	3.9	6.0	5.3	5.1	5.6	6.2	5.1	5.5
Nd	17	25	23	22	24	27	22	24
Sm	4.0	6.0	5.3	5.0	5.4	6.2	5.0	5.4
Eu	1.33	1.84	1.64	1.59	1.74	1.95	1.60	1.70

(*continued on next page*)

Table 1 (*continued*)

Suite	L-Ti							
Sample	T BAS-37	T BAS-38	WR-02B	WR-09	WR-16	WR-29	WR-32	WR-62
Gd	4.3	6.5	5.5	5.5	6.1	7.0	5.6	5.9
Tb	0.694	1.03	0.892	0.867	0.958	1.10	0.880	0.937
Dy	4.3	6.3	5.1	5.0	5.5	6.5	5.1	5.5
Ho	0.913	1.36	1.12	1.15	1.27	2.45	1.46	1.62
Er	2.4	3.7	3.0	3.1	3.4	3.9	3.1	3.3
Tm	0.353	0.533	0.450	0.454	0.489	0.580	0.459	0.500
Yb	2.18	3.3	2.75	2.80	2.94	3.5	2.86	3.0
Lu	0.324	0.496	0.423	0.437	0.464	0.551	0.447	0.480
Hf	2.85	4.2	3.8	3.8	4.1	4.6	3.9	4.0
Ta				0.901	0.818	0.935	0.781	0.811
Pb	2.56	3.4	2.56	2.99	3.2	3.6	2.87	3.2
Th	0.231		2.12	2.14	2.36	2.59	2.19	2.29
U	0.356	0.448	0.403	0.415	0.541	0.494	0.427	0.454

Suite	H-Ti								
Sample	AJ-49	AJ-70	LG - 147	LG-46B	LG-46 T	LL - 082	LL - 131	LL - 136	LL-32
SiO_2	48.55	48.48	48.08	48.95	47.40	48.29	48.26	48.54	48.87
TiO_2	3.69	3.75	3.67	3.78	4.06	3.87	3.96	3.83	3.90
Al_2O_3	12.34	12.34	12.23	12.85	11.82	12.58	12.54	12.43	12.56
Fe_2O_3	1.90	1.91	1.90	1.83	1.96	1.82	1.79	1.83	1.84
FeO	14.08	14.14	14.07	13.54	14.53	13.52	13.25	13.55	13.67
MnO	0.22	0.20	0.21	0.20	0.19	0.19	0.21	0.17	0.17
MgO	4.54	4.69	5.44	4.85	5.34	4.64	4.63	4.80	4.72
CaO	8.73	8.76	8.95	9.03	9.14	8.99	8.89	8.80	9.00
Na_2O	2.35	2.40	2.42	2.49	2.27	2.42	2.41	2.49	2.43
K_2O	1.08	1.23	1.18	1.27	1.17	1.14	1.36	1.27	1.25
P_2O_5	0.38	0.35	0.35	0.34	0.33	0.38	0.34	0.36	0.36
LOI	1.32	1.04	1.02	0.76	0.80	1.34	1.32	1.22	0.96
Total	99.17	99.28	99.51	99.89	99.01	99.18	98.96	99.30	99.73
Mg#	0.45	0.45	0.44	0.46	0.46	0.47	0.42	0.41	0.47
Rb	21	24	23	24	23	15	25	23	25
Sr	447	416	479	428	403	481	462	446	435
Y	34	30	31	30	32	31	30	30	34
Zr	218	208	260	195	188	264	255	259	209
Nb	21	21	20	20	19	21	20	20	20
Cs	0.730	0.115	0.153	0.529	0.452	0.191	0.159	0.149	1.26
Ba	516	455	382	409	405	391	397	379	442
La	30	28	26	27	26	28	27	27	29
Ce	64	59	62	57	54	67	63	65	60
Pr	8.4	7.6	8.0	7.5	7.2	8.6	8.1	8.4	7.8
Nd	36	33	34	32	31	37	35	36	34
Sm	7.8	7.1	7.5	7.0	6.8	8.0	7.5	7.8	7.3
Eu	2.47	2.30	2.35	2.27	2.20	2.51	2.36	2.43	2.42
Gd	6.7	6.3	7.0	6.1	6.1	7.4	7.1	7.3	7.5
Tb	1.12	1.04	1.07	1.01	1.02	1.13	1.08	1.11	1.09
Dy	6.2	5.7	5.8	5.6	5.7	6.1	5.8	6.0	6.0
Ho	1.24	1.13	1.18	1.12	1.14	1.24	1.19	1.23	2.11
Er	3.4	3.1	3.1	3.0	3.1	3.2	3.1	3.2	3.3
Tm	0.474	0.436	0.433	0.426	0.432	0.451	0.429	0.449	0.461
Yb	2.79	2.54	2.54	2.53	2.54	2.64	2.55	2.67	2.71
Lu	0.418	0.380	0.381	0.377	0.387	0.401	0.379	0.398	0.419
Hf	5.7	5.4	5.4	5.1	4.9	5.6	5.4	5.6	5.4
Ta	1.73	2.75		1.46	1.31				1.31
Pb	4.0	3.7	3.3	3.6	3.4	3.4	3.4	3.4	3.6
Th	2.93	2.73	2.62	2.59	2.44	2.76	2.69	2.83	2.65
U	0.565	0.524	0.504	0.545	0.496	0.521	0.569	0.560	0.579

2011 to 28 January 2011 (samples TBAS-4, LG 46.BASE, WR32) and 28 April 2011 to 30 April 2011 (samples L1, O-19, CH-6) in the Cadmium-lined B-1 CLICIT facility, a TRIGA-type reactor, Oregon State University, USA. All ages are reported using the decay constants of Steiger and Jäger (1977). Samples were analysed by laser $^{40}Ar/^{39}Ar$ heating following procedures detailed in Vasconcelos et al. (2002). Before analysis, the rock grains and fluence monitors were baked-out under vacuum at ~200 °C for ca. 12 h. Each sample was heated incrementally with a continuous-wave Ar-ion laser with a 2 mm wide defocused beam. The fraction of gas released was cleaned through a cryocooled cold-trap ($T = -125$ °C) and two C-50 SAES Zr-V-Fe getters and analysed for Ar isotopes in a MAP215–50 mass spectrometer equipped with a third C-50 SAES Zr-V-Fe getter. Full system blanks and air pipettes were determined before and after each sample. The data were corrected for mass discrimination, nucleogenic interferences, and atmospheric contamination following the procedures in Vasconcelos et al. (2002), using the software "MassSpec Version 7.527" developed by Alan Deino of the Berkeley Geochronology Centre, USA. A $^{40}Ar/^{36}Ar$ value of 298.56 ± 0.31 for atmospheric argon was used for the calculation of the mass spectrometer discrimination (Lee et al., 2006). J-factors for each Al-disk were determined by the laser total fusion analyses of 15 individual aliquots of neutron fluence monitor, each aliquot consisting of one to three crystals of Fish Canyon sanidine. The mass spectrometer sensitivity was calculated based on the analysis of an air pipette (1.634×10^{-13} mol

Table 2
Alto Diamantino basalts isotopic ratios for Sr and Nd.

Sample	Suite	Rb ppm	Sr ppm	$^{87}Sr/^{86}Sr$	$^{87}Rb/^{86}Sr$	$^{87}Sr/^{86}Sr_{(134)}$	Sm ppm	Nd ppm	$^{143}Nd/^{144}Nd$	$^{147}Sm/^{144}Nd$	$\varepsilon Nd_{(134)}$	T_{DM} Age (Ma)
Wr-16	L-Ti	27	290	0.706385(36)	0.2668	0.705886	5.5	24.0	0.512389(8)	0.1373	−3.8	1026
Wr-29	L-Ti	39	277	0.706370(33)	0.4110	0.705603	6.2	26.9	0.512392(8)	0.1401	−3.8	1048
Wr-32	L-Ti	19	287	0.706132(15)	0.1908	0.705776	5.0	21.9	0.512399(8)	0.1392	−3.7	1029
LL3	L-Ti	18	267	0.706038(11)	0.1901	0.705683	4.7	20.2	0.512391(5)	0.1409	−3.9	1057
LL70	L-Ti	22	290	0.706360(32)	0.2160	0.705957	5.1	22.1	0.512391(8)	0.1401	−3.9	1050
LL08	L-Ti	17	295	0.706310(41)	0.1635	0.706004	5.1	21.8	0.512400(6)	0.1424	−3.7	1059
AJ-49	H-Ti	21	447	0.705817(42)	0.1353	0.705564	7.8	35.9	0.512358(9)	0.1307	−4.3	1009
AJ-70	H-Ti	24	416	0.705790(19)	0.1640	0.705484	7.1	32.7	0.512360(6)	0.1311	−4.3	1009
LL32	H-Ti	25	435	0.705835(16)	0.1697	0.705518	7.3	33.8	0.512347(7)	0.1306	−4.5	1021
LG46B	H-Ti	24	428	0.705961(42)	0.1618	0.705659	7.0	32.0	0.512345(5)	0.1315	−4.6	1032

^{40}Ar) on the Faraday detector (4.257 mV) equipped with a 1×10^{11} Ohms resistor, yielding a Faraday sensitivity of 3.84×10^{-9} mol/nA. The current multiplier sensitivity measured on a Balzers 217 Electron Multiplier, operated with a gain of ~145,000 is $\sim 4.5 \times 10^{-14}$ mol/nA. All results are presented at 2 sigma uncertainty levels. Data of each run are reported in Supplementary Material 1.

4.2. Bulk major and trace elements

Bulk rock major and trace elements were analysed at the laboratories of the Departamento de Mineralogia e Geotectônica, Instituto de Geociências, Universidade de São Paulo. (Brazil). Major elements were analysed at the X-ray fluorescence laboratory by wavelength dispersive X-ray spectrometry (Philips PW 2400) using fused glass discs according to procedures described in Mori et al. (1999). Accuracy was better than 2%. We used Inductively Coupled Plasma-Mass Spectrometry (ICP-MS) to determine trace elements in selected samples. Samples were dissolved in Parr bombs in a microwave furnace as described by Navarro et al. (2008). Accuracy, determined with respect to the reference standards BHVO-2 and BRP-1, was between 0.5 and 2%. Data are reported in Table 1.

4.3. Sr and Nd isotopes

Sm-Nd and Rb-Sr whole-rock isotopic analyses were carried out at the Geochronological Research Center (CPGeo) of the University of São Paulo following the procedure detailed in Sato et al. (1995). The powered samples were dissolved with a $^{149}Sm/^{150}Nd$ mixed spike solution and a combination of hot suprapure HF and HNO_3 acids in Teflon vessels. Rare earth elements including Sm and Nd were extracted using cationic exchange columns filled with AG50W-X8 resin (200–400 mesh). Sm and Nd were separated using a secondary hydrogen di-Ethylhexyl phosphate (HDEHP) coated Teflon powder column.

The Sm and Nd concentrations and isotopic ratios of the samples were measured on a VG Iso-mass 354 automated mass spectrometer using five Faraday collectors in static mode. The laboratory blanks yielded maximum values of 0.4 ng for Nd and 0.7 ng for Sm. The La Jolla standard yielded a mean $^{143}Nd/^{144}Nd$ ratio of 0.511857 ± 15 ($n = 46$; 1σ level). All the $\varepsilon Nd_{(t)}$ initial values were calculated at 134 Ma.

Rb and Sr contents were determined by X-ray fluorescence spectrometry (precision >2.0%) in powdered samples. The isotope dilution technique was applied to the samples with Rb contents lower than 44 ppm for better precision of the measurements compared to the X-ray fluorescence data. The average precision (1σ level) for the calculated $^{87}Rb/^{86}Sr$ ratios by isotope dilution was 1.4%. Sm-Nd and Rb-Sr isotopic determination were carried out by Isotope Dilution Thermal Ionization Mass Spectrometry (ID-TIMS) using a VG-354 multicollector and single collector mass spectrometers of the CPGeo. The $^{87}Sr/^{86}Sr$ ratios were normalized to $^{86}Sr/^{88}Sr = 0.1194$. The final quoted errors are external ones (1σ level) based on replicate analyses of $SrCO_3$ NBS-987, which yielded a mean ratio of 0.710254 ± 0.000022 (2σ level). The overall blank for the chemical procedure was 4 ng for Sr during the period of the analyses. Decay constants are those recommended by Nebel et al. (2011). Data are reported in Table 2.

5. Results

5.1. Geochronology

We dated three samples – TBAS-01, LG-46 (high-Ti) and WR-32b (low-Ti) – by whole-rock laser incremental heating $^{40}Ar/^{39}Ar$ analysis.

Both grains of sample TBAS-01 produced similar age spectra with plateau ages (134.5 ± 2.7 and 134.07 ± 0.82 Ma) compatible at the 2σ confidence level (Fig. 2a). The first steps for both grains show a minor low temperature discordance probably related to ^{40}Ar loss due to alteration. The following low temperature steps for both grains yield slightly older ages probably due to minor ^{39}Ar recoil losses or the presence of some excess argon. The isochron age of 134.22 ± 0.95 Ma, with an atmospheric intercept of 299.1 ± 4.8, is compatible at the 2-sigma confidence level with the plateau ages (Fig. 2b). An age probability diagram plotted from the best contiguous steps from both grains yields a maximum probability peak of 134 Ma (Fig. 3), and defines a mean-weighted age of 134.18 ± 0.8 Ma, which is also compatible at the 2σ level with the plateau ages. Our best age estimates for sample TBAS-01 is the isochron age of 134.22 ± 0.95 Ma (Fig. 2).

The two grains from sample LG-46 yielded nearly identical spectra with compatible plateau ages of 134.29 ± 0.74 and 133.93 ± 0.82 Ma. The initial steps for both grains show evidence for either minor recoil or some excess argon in the sample. An isochron for most of the plateau steps defines an age of 133.89 ± 0.67 Ma with an atmospheric $^{40}Ar/^{36}Ar$ intercept at 281 ± 29 Ma. The isochron and plateau ages are compatible at the 2σ confidence level (Fig. 2c,d). An age probability diagram plotted from the best contiguous steps from both grains yields a maximum probability peak of 134 Ma, and defines a mean-weighted age of 133.78 ± 0.67 Ma, compatible at the 2σ level with the plateau and isochron ages (Fig. 3). Our best age estimates for sample LG-46 is the isochron age of 133.89 ± 0.67 Ma.

Two grains from sample WR-32b also produced nearly identical spectra with compatible plateau ages of 132.98 ± 0.73 and 133.00 ± 0.82 Ma (Fig. 2e). Once again, the initial steps for both grains show evidence for either minor recoil or some excess argon in the sample. The isochron age of 132.77 ± 0.77 Ma is compatible at the 2σ confidence level with the plateau ages (Fig. 2f). The $^{40}Ar/^{36}Ar$ intercept of 343 ± 17 Ma suggests minor excess argon in the sample. The age probability diagram plotted shows that the best contiguous steps yield a maximum probability peak of 132.6 Ma and a mean-weighted age of 132.99 ± 0.63 Ma (Fig. 3). The best age estimates for sample WR-32b is the isochron age of 132.77 ± 0.77 Ma.

Using the new age for the Fish Canyon sanidine (28.294 Ma) and new values for the K-decay constants proposed by Renne et al. (2011), the three preferred isochron ages of 134.22 ± 0.95 Ma (TBAS-01), 133.89 ± 0.67 Ma (LG-46), and 132.77 ± 0.75 Ma (WR-32b) recalculate to 134.7 ± 1.0 Ma (TBAS-01), 134.3 ± 0.8 Ma (LG-46), and 133.2 ± 0.8 Ma (WR-32b). Owing to the recently revised ages for the PEMP compiled

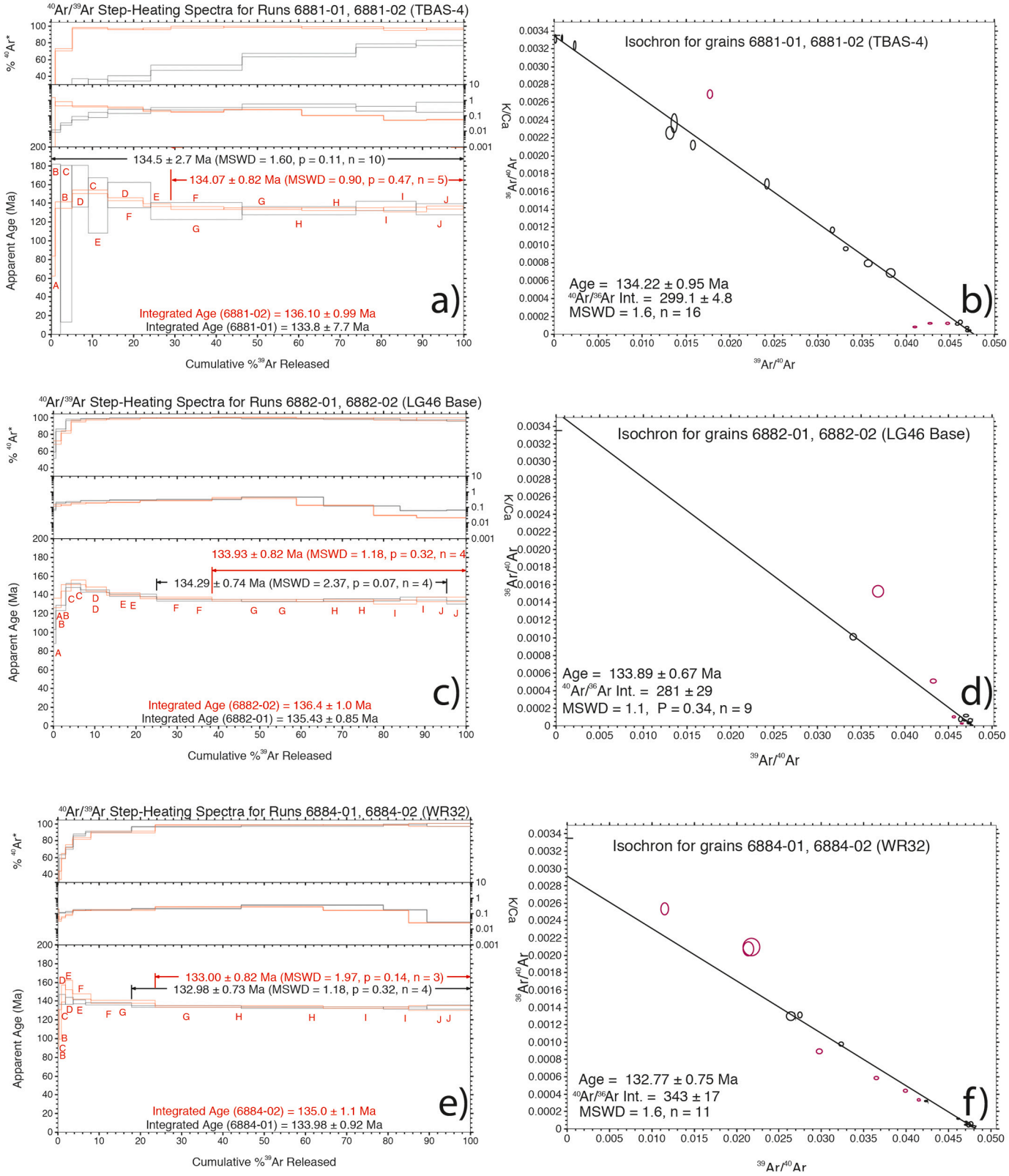

Fig. 2. $^{40}Ar/^{39}Ar$ results for samples T-BAS4, LG46 and WR32. Fig. 2a, c and e show step-heating spectra where plateaus correspond to three or more contiguous steps with >50% ^{39}Ar released from the sample. MSWD – mean square weighted deviation. Fig. 2b, d and f are Ar-Ar isochrone ages.

by Gomes and Vasconcelos (2021), we will be using the ages recalculated with the values of Renne et al. (2011).

5.2. Petrography and geochemistry

The analysed samples are medium to fine grained, composed mainly of plagioclase (andesine-labradorite) and clinopyroxene (mainly

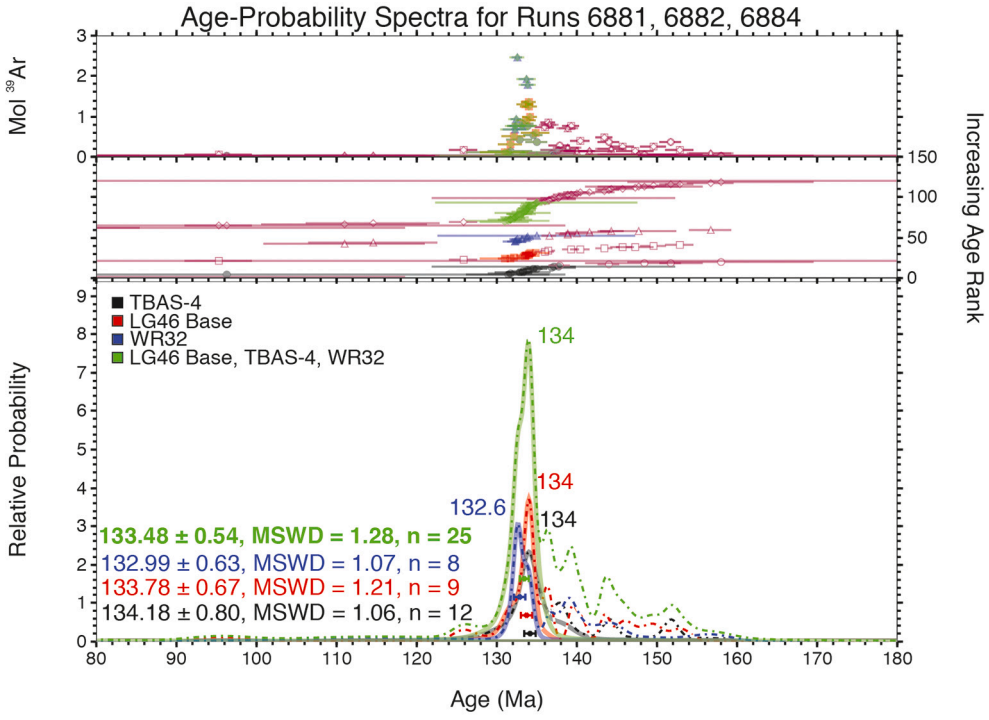

Fig. 3. Age probability density plot for each run of Ar isotopic analysis.

augite). Pigeonite occurs in some samples, as well as biotite and olivine, which is partially replaced by iddingsite. Opaque minerals (magnetite and ilmenite) and apatite are common accessory minerals. Sub-ophitic texture is largely predominant, but ophitic or intergranular textures are also present in some samples. In this case, micro-phenocrysts of plagioclase, which in few cases become phenocrysts up to 1 cm, can occur in a fine-grained groundmass.

The Alto Diamantino lavas plot in the basalt field in the SiO_2 versus $Na_2O + K_2O$ diagram (TAS diagram, Le Bas et al., 1992; Fig. 4a), pointing to a tholeiitic affinity in the AFM diagram (Fig. 4b). Tholeiitic basalts can be divided in a low-Ti group (L-Ti; $TiO_2 < 3$ wt%, samples between 1.79 and 2.49 wt%) and in a high-Ti group (H-Ti; $TiO_2 > 3$ wt %, samples between 3.67 and 4.06 wt%) (Fig. 5, Table 1). Besides TiO_2, the H-Ti lava suite is richer in FeO_T, Na_2O, K_2O, P_2O_5 and all incompatible elements with respect to the L-Ti lava suite (Table 1; Fig. 6) which is enriched in SiO_2 (Figs. 4 and 5). The two groups are characterized by Mg# values (calculated as $Mg^{2+}/(Mg^{2+}+Fe_T^{2+})$ mol) varying from 0.38 to 0.51 in the L-Ti and from 0.36 to 0.40 in the H-Ti lavas. The significant differences displayed by the two suites in terms of Zr vs Rb, Pb, Y and Yb additionally support the distinction in the L-Ti and H-Ti suites (Table 3). L-Ti lavas have average Zr/Rb (7.62), Zr/Pb (48.74), Zr/Y (4.47), and Zr/Yb (50.45) higher than H-Ti lavas (Zr/Rb = 10.17, Zr/Pb = 64.83, Zr/Y = 7.31, and Zr/Yb = 87.49). Also, L-Ti and H-Ti have similar Ba/La, Zr/Nb, and La/Sm ratios, but H-Ti has higher Zr/Y, Ce/Y, La/Yb, Ti/Zr and Ti/Y and lower Ba/Nb, La/Nb and Th/Ta ratios (Table 3).

Chondrite-normalized (Lyubetskaya and Korenaga, 2007) rare earth elements (REE) patterns for both suites are fractionated with light REE (LREE) enrichments over heavy REE (HREE) (Fig.6a). H-Ti basalts, however, are characterized by higher LREE abundances and a more fractionated trend (La_N/Yb_N between 7.0 and 7.5 and between 4.1 and 4.9, respectively) compared to L-Ti lavas. Trace elements show similar geochemical affinity within each group (Fig. 6b). Multielement diagrams (primitive mantle-normalized; PM, McDonough and Sun, 1995) of both groups display similar patterns but again H-Ti lavas have higher abundances (Figs. 6b and 7). Both suites show prominent Ba peaks, negative Nb, Ta, Sr and Zr anomalies, enrichment in LREE and MREE with respect to HREE, but the H-Ti basalts show a more pronounced positive Ti anomaly and a negative Pb anomaly not present in the L-Ti suite (Figs. 6b and 7). The H-Ti lavas also show variable Rb and Ta contents while two samples do not show Zr negative anomaly (Figs. 6b and 7).

When compared to the Atlantic *E*-MORBs, the two suites have very similar Zr/Y, Ti/Zr, Ti/Y, and Zr/Nb ratios (Klein, 2004; Table 3), whereas Ce/Y, Ba/Nb, La/Nb, Ba/Nb, Th/Ta and La/Sm ratios are higher. The Ce/Y, La/Nb, Zr/Nb and Zr/Y ratios are similar to those from the lower crust (Hacker et al., 2015), which displays higher Ba/Nb and Ba/La ratios (Table 3). Finally, the H-Ti suite has very high Ti/Y and Zr/Y ratios, similar to the OIB average pattern (Sun and McDonough, 1989; Table 3).

5.3. Sr and Nd isotopes

$^{87}Sr/^{86}Sr$ and $^{143}Nd/^{144}Nd$ isotopic ratios were recalculated to 134 Ma, which is the mean formation age according to our data and recent literature (Gomes and Vasconcelos, 2021; Janasi et al., 2011; Thiede and Vasconcelos, 2010). The recalculated values support the classification in L-Ti and H-Ti suites, initially based on major and trace element data. L-Ti basalts have $^{87}Sr/^{86}Sr_{(134)}$ ratios ranging from 0.705603 to 0.706004 and $^{143}Nd/^{144}Nd_{(134)}$ from 0.512268 to 0.512277 (Fig. 8) with $\varepsilon Nd_{(134)}$ between −3.9 and − 3.7 (Table 2). H-Ti basalts show ratios in the range 0.705484–0.705659 for $^{87}Sr/^{86}Sr_{(134)}$ and in the range of 0.512230–0.512245 for $^{143}Nd/^{144}Nd_{(134)}$ (Fig. 8) with $\varepsilon Nd_{(134)}$ between −4.3 to −4.6 (Table 2).

6. Discussion

6.1. The Alto Diamantino basalts: The westernmost expression of the PMP

The Alto Diamantino basalts based on their physical appearance and stratigraphic position were attributed to the Serra Geral Formation and the PMP (Barros et al., 1982; Lacerda Filho et al., 2004). Our geochronological results for three distinct samples – 134.7 ± 1.0 Ma (TBAS-01), 134.3 ± 0.8 Ma (LG-46), and 133.2 ± 0.8 Ma (WR-32b) – confirm that

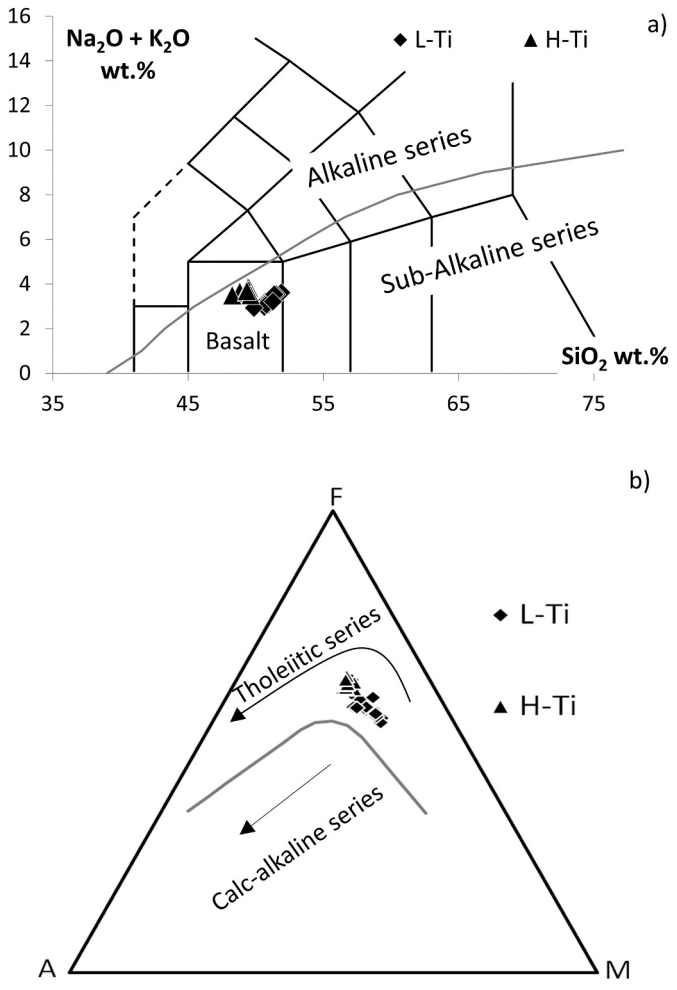

Fig. 4. A) Total Alkali vs Silica and AFM classification diagrams. B) AFM diagram.

the Alto Diamantino basalts are indeed coeval with the PMP province with ages between the accepted range of formation of the PMP of 135.5 ± 0.4 and 132.0 ± 0.1 (see Gomes and Vasconcelos, 2021).

The occurrence in Alto Diamantino of two – low- and high-Ti –basaltic suites, and their geochemical composition are also similar to other PMP magmatic extrusive units and suggest a genetically related magmatic origin. Thus, the Alto Diamantino basalt flows represent the extreme northwestern occurrence of the PMP at the border of the Paraná Basin.

Subdivision based on TiO_2 content is common use for PMP magmatics and other continental flood basalts (e.g., Central Atlantic Magmatic Province; Oliveira et al., 2018). The most utilized PMP classification of Peate et al. (1992) divides the two magmatic series in six compositional groups, namely Gramado, Esmeralda and Ribeira (L-Ti); Paranapanema, Pitanga and Ubirici (H-Ti). The classification is based on TiO_2 abundance, Ti/Y and Ti/Zr ratios and Sr isotopic composition. This classification has been largely employed in its original form (e.g., Machado et al., 2018), using only some parameters (e.g., H-Ti >2 wt% and L-Ti <2 wt%; Marques et al., 2016; for the Southern Espinhaço dykes) or adding new ones (e.g., De Min et al., 2018, added La_N/Sm_N and La_N/Yb_N ratios to the classification of Peate et al., 1992).

Taking into account the overall distribution of the geochemical parameters of the Alto Diamantino basalts, the subdivision in two suites can be set for TiO_2 of 3.00 wt% and Ti/Y of 450. Other geochemical parameters that well discriminate the two series are the Zr/Y (between 3.78 and 6.01 for L-Ti and 5.54–8.60 for H-Ti) and the Nb/Yb ratios (between 3.82 and 5.82 for the L-Ti and 5.60–8.31 for the H-Ti). Considering the classification of Peate et al. (1992), the lava flows from Alto Diamantino could be classified as Pitanga (H-Ti) while the L-Ti are mainly Ribeira (Fig. 9) with one sample classified as Esmeralda (Fig. 9). Three samples could be classified as Paranapanema based on TiO_2 (2.40–2.49 wt%) however, due to their geochemical characteristics and to the fact they are near the TiO_2 limit for Ribeira (TiO_2 of 1.5–2.3 wt%; Peate et al., 1992) we include them in the L-Ti group. Trace elements compositions of the three Paranapanema-type and the one Esmeralda are identical to the Ribeira ones (Fig. 6b). This reinforce the inclusion of these samples in the L-Ti group with the only observable difference a slightly more pronounced positive Ti-anomaly (Fig. 6b). Isotopically, L-Ti are similar to Ribeira (Fig. 8) as also observed in multielement diagrams (Fig. 7).

Based on geochemical features (e.g. the low Mg#), Alto Diamantino basalts show a differentiated nature. The enrichments in Fe, alkali elements and P and the lower Mg content (and thus lower Mg#) suggest that H-Ti lavas are more evolved compared to L-Ti lavas. Differences in major element composition of the two suites cannot be explained by different degrees of fractionation from a unique melt (Fig. 5), thus suggesting different mantle sources and/or melts evolution. This hypothesis is confirmed by different trends of the CaO/Al_2O_3 ratio at increasing SiO_2 of the two suites. CaO/Al_2O_3 ratio linearly decreases in the H-Ti basalts, thus suggesting a melt evolution controlled by clinopyroxene fractional crystallization. Instead, CaO/Al_2O_3 is scattered for the L-Ti, pointing to different mineral fractionation. Moreover, the H-Ti suite is enriched in all incompatible elements (Fig. 6b), except for the HREE, and it displays a more prominent positive Ti anomaly and a more negative Pb anomaly compared to L-Ti basalts. Both groups are enriched in LILE and LREE with respect to HSFE, MREE and HREE, but several ratios show significant differences (Table 3).

Areal distribution of the L-Ti and H-Ti basalts (in the southeast and northwest, respectively) suggests a stratigraphic order of the two suites. Given that the northern PMP units form a N-S 'synform' structure with lava flows thickness increasing towards the centre of the basin (i.e., southeast; Machado et al., 2015; Fig. 13 from Gomes and Vasconcelos, 2021), L-Ti basalts in Alto Diamantino seem to be on top of H-Ti basalts. If this observation is correct, this represents a unique case in the PMP: H-Ti units in fact commonly overlap L-Ti basalts in the central and southern part of PMP (Gomes and Vasconcelos, 2021; Peate et al., 1992). Peate et al. (1992) reported Ribeira (L-Ti) overlying Esmeralda-type basalts in the GO borehole (central PMP) but below Pitanga (H-Ti) type, while Petrini et al. (1987), notwithstanding this was also a secondary interpretation from Peate et al. (1992), reported them above H-Ti Paranapanema-type (CB borehole, northern PMP). Machado et al. (2015) reported Ribeira-type basalts at the west margin of the northern sector of Parana overlaid towards the centre by Pitanga-type ones. The finding of Ribeira-type basalts at the top of Pitanga-type basalts in Alto Diamantino suggests that the occurrence of H-Ti basalts is not always at the top of the PMP. This possibly means that the production of high and low Ti suites in the PMP is not a time-dependent process.

6.2. *Constraints on the Alto Diamantino mantle source and degree of melting*

The evolved nature of the Alto Diamantino basalts (and also of other PMP basalts) requires special attention when investigating the nature of the PMP mantle sources. Estimations of the primitive composition of the melts are strongly dependant on KDs and knowledge of mineral fractionation, assimilation and contamination processes. Another approach is to evaluate elemental differentiation caused by these processes and use ratios of elements not affected (see e.g. Pfänder et al., 2007). To do this, we check whether or not the slope (m) of the equation describing the variation of the logarithmic element concentration is close as possible to 1.

As previously discussed, the geochemical differences between the H-Ti and L-Ti series are likely related to the different composition of the

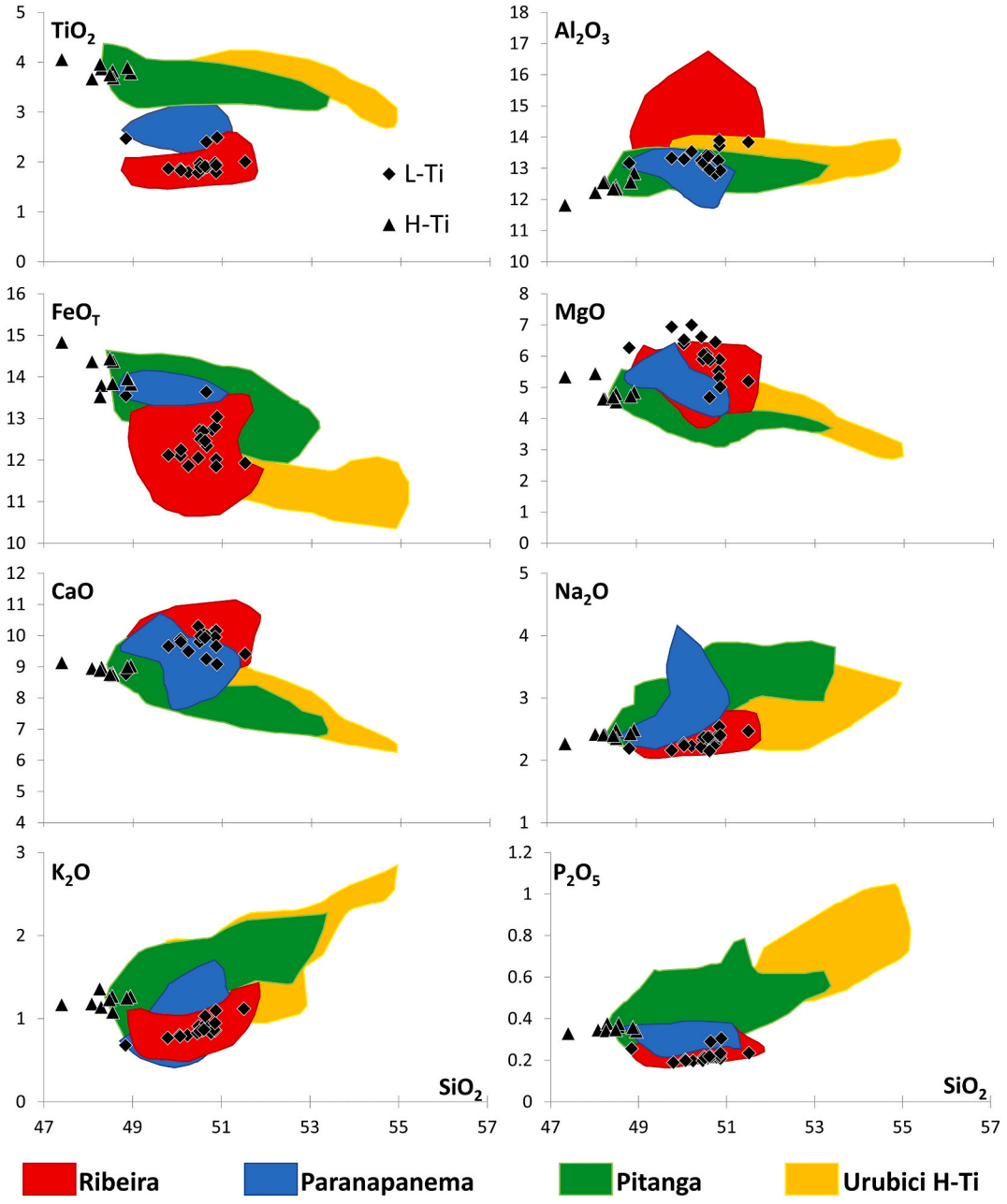

Fig. 5. Major elements variations (reported as oxide wt%) vs SiO_2. For comparison, basalts and rhyolites from the alkaline Mesozoic magmatism of the PMP are reported: Pitanga, Paranapanema and Ribeira basalts (GEOROC database http://georoc.mpch-mainz.gwdg.de/georoc/) and Urubici H-Ti basalts (Peate et al., 1999).

melts either primarily inherited from the mantle source or acquired secondarily through AFC or mixing processes during melt differentiation. Isotopic values and Ba enrichments in the Alto Diamantino basalts suggest a crustal component as possible 'contaminant' of the melts. However, a lack of co-variation between isotopic and elemental data (e.g., $^{87}Sr/^{86}Sr_{(134)}$ vs 1/Sr, SiO_2, P_2O_5/K_2O or La_N/Yb_N; Fig. 10) indicates that contamination by hydrothermal activity, AFC or mixing during melt ascent within the continental crust was absent or negligible. Moreover, Pb, is also a good indicator of crustal assimilation during magma ascent because it could be easily enriched. Absence of positive Pb anomalies (Fig. 6b) rule out this possibility. Thus, the crustal component in the melts must be a primary feature of the mantle source, and can be explained by a metasomatized mantle column. This is also suggested by Ce/Pb and Nb/U ratios and by Nb/Ta and Zr/Hf ratios (Fig. 9; ratios correlated with $m > 0.8$).

Absence of crustal assimilation by H-Ti basalts was reported for the central (De Min et al., 2018) and northern (Rocha-Júnior et al., 2013) PMP. Conversely, crustal assimilation is considered to have played an important role for the evolution of L-Ti basalts in the central PMP (De Min et al., 2018). The Alto Diamantino L-Ti group contrasts this evidence (Figs. 9 and 10). Although age estimations could not discriminate the geographical migration (if occurred) of the flood basalt eruptions (Gomes and Vasconcelos, 2021), a northward migration of the magmatism due to the northward overlapping of the magma types has been suggested (Peate et al., 1992). The absence of crustal assimilation in Alto Diamantino (and for L-Ti basalts in particular) could be possibly explained by the position of the area at the northwestern border of the Paraná basin where crustal thickness is higher. However, the rocks, being near the Brasilia orogenic belt, have a restitic character and the heating of the main PMP activity had a minor impact on the crust.

Several hypotheses in the literature account for the thermal anomaly related to the origin of the PMP: mantle-plume activity of the Tristan da

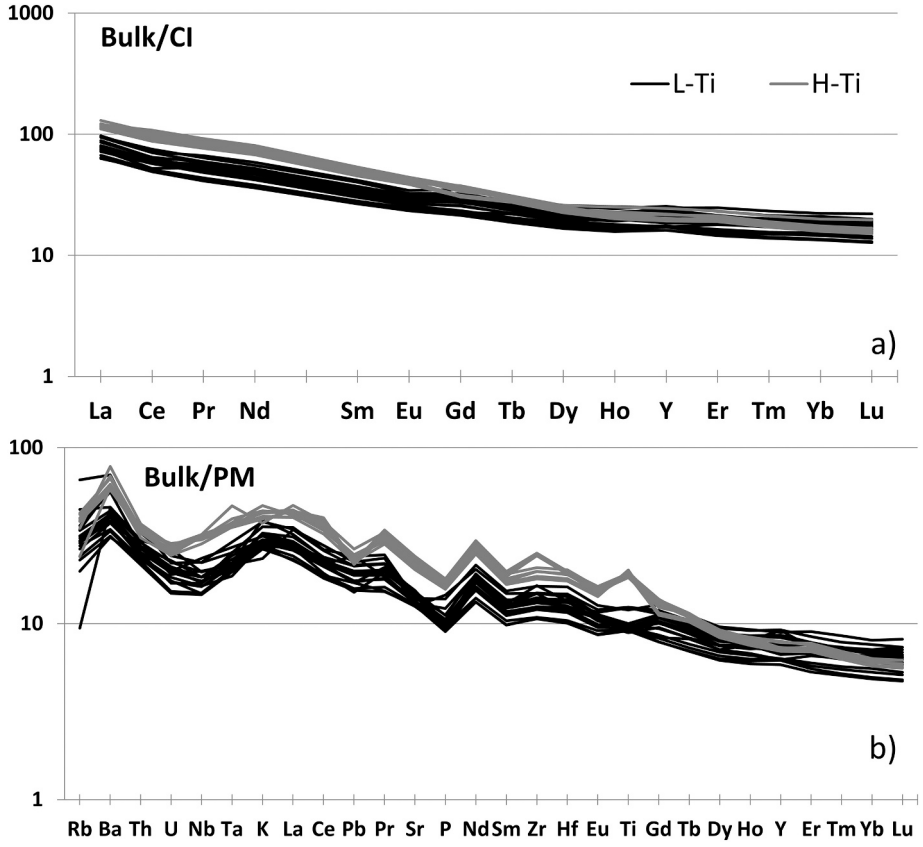

Fig. 6. A) REE diagram of Alto Diamantino bulk rock normalized to Chondrite-I (Lyubetskaya and Korenaga, 2007); B) multielement diagrams of Alto Diamantino bulk rock normalized to the Primitive Mantle composition recalculated from Pyrolite (PM; McDonough and Sun, 1995).

Table 3
Comparative ratios of L-Ti and H-Ti basalts (averages) and different reservoirs: N-MORB and OIB are from Sun and McDonough (1989), Atlantic *E*-MORB is from Klein (2004), Tristan da Cunha is an average from the GEOROC database (http://georoc.mpch-mainz.gwdg.de/georoc/), Lower Continental Crust (LCC) is from Rudnick and Gao (2003) and GLOSS is from Plank and Langmuir (1998). *m* is the slope of the linear equation calculated on the logarithmic values of trace elements.

Source	L-Ti	*m*	H-Ti	*m*	N-MORB	E-MORB	OIB	Tristan da Cunha	LCC	GLOSS
La/Sm	3.72	0.97	3.72	0.49	0.95	2.63	3.70	8.05	4.00	4.98
La/Yb	6.64	0.99	10.59	0.61	0.82	4.29	17.13	27.00	5.33	10.43
La/Nb	1.54	0.94	1.37	0.46	1.07	1.03	0.77	0.79	1.60	3.22
Ba/La	15.15	0.52	15.18	0.40	2.52	10.70	9.46	11.75	32.38	26.94
Ba/Rb	15.21	1.08	18.67	−0.23	11.25	13.90	11.29	12.33	15.24	13.57
Ba/Nb	23.35	0.49	20.78	0.16	2.70	10.98	7.29	9.22	51.80	86.80
Zr/Nb	11.70	0.68	11.31	0.09	31.76	11.96	5.83	3.89	17.20	14.54
Zr/Y	4.47	0.78	7.31	−0.10	2.64	4.62	9.66	10.33	5.38	4.36
Zr/Pb	48.74	0.52	64.83	−0.21	246.67	141.05	87.50	62.72	28.67	6.53
Zr/Rb	7.62	1.47	10.17	−0.02	132.14	15.14	9.03	5.20	5.06	2.27
Zr/Yb	50.45	0.85	87.49	0.04	24.26	50.00	129.63	133.81	57.33	47.10
Ti/Zr	84.33	0.52	100.56	−0.82	102.70	81.87	61.43	70.62	57.16	28.59
Ti/Y	377.08	0.90	734.92	−0.03	271.43	378.31	593.10	729.55	307.25	124.73
Rb/Sr	0.08	0.11	0.14	−0.06	0.01	0.05	0.05	0.05	0.05	0.17
Th/Ta	2.61	0.55	1.86	1.50	0.91	1.39	1.48	1.54	2.17	10.97
Ce/Y	1.19	0.86	1.96	0.02	0.27	0.90	2.76	4.57	1.25	1.92
Ce/Pb	12.93	1.01	17.35	−0.04	24.54	27.37	25.00	27.76	6.67	2.88
Nb/Th	5.60	1.06	7.50	1.01	18.74	10.47	12.00	10.36	3.85	1.29

Cunha plume (Ewart et al., 1998; Gibson et al., 2005; Hoernle et al., 2015), heating of a heterogeneous sublithospheric mantle by the Tristan da Cunha plume (Marques et al., 1999; Peate et al., 1999) or melting of heterogeneous sublithospheric mantle unrelated to the plume (De Min et al., 2018; Ernesto et al., 2002; Rocha-Júnior et al., 2013). The isotopic composition of the two suites points towards the involvement of the EM-I end-member (Fig. 8). EM-I basalts form a very large isotopic field and the origin of this end-member is still very much debated and includes: a) derivation from near-primitive lower-mantle (e.g. Roden et al., 1994); b) metasomatism induced by carbonatitic melts or peridotite devolatilization (Eiler et al., 1995); c) recycling of oceanic crust (e.g. Eisele et al., 2002; Woodhead et al., 1993), subduction-modified mantle wedge (Kempton et al., 2002) or lower continental crust (e.g. Frey et al., 2002; Willbold and Stracke, 2006); d) mixing with subcontinental lithosperic mantle (e.g. Gibson et al., 2005; Hawkesworth et al., 1986).

The hypothesis of a metasomatized mantle source is consistent with low Nb and Ta abundances compared to Th and La (e.g. Nb_N/La_N or Nb_N/Th_N ratios <1; Nb-La $m = 0.78–0.79$, Nb-Th $m = 1.01–1.06$), with

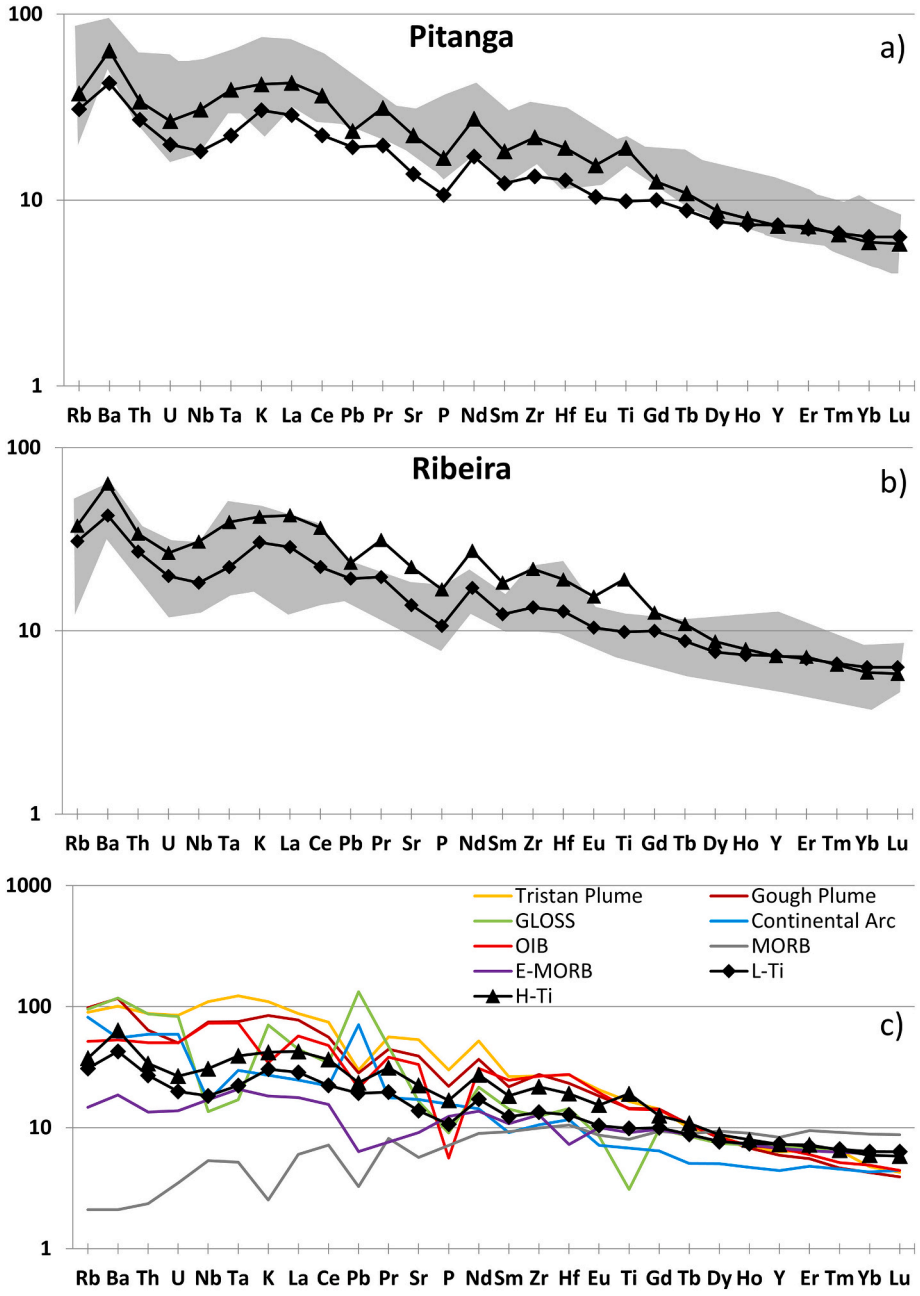

Fig. 7. Comparison of average L-Ti and H-Ti Alto Diamantino basalts with A) Pitanga basalts (Rocha-Júnior et al., 2013); B) Ribeira basalts (Rocha-Júnior et al., 2020); C) geochemical reservoirs: Tristan Plume and Gough Plume (averages based on data from the GEOROC database http://georoc.mpch-mainz.gwdg.de/georoc/), GLOSS (Plank and Langmuir, 1998), OIB (Sun and McDonough, 1989) MORB (Hofmann, 1988) and Atlantic *E*-MORB (Klein, 2004). All multielement diagrams are normalized to the Primitive Mantle composition recalculated from Pyrolite (PM; McDonough and Sun, 1995).

the enrichment in incompatible elements as LREE and LILEs and with the Ba positive anomaly in the Alto Diamantino basalts (Figs. 6, 7 and 9). Moreover, in the Nb/Ta vs Zr/Hf diagram (Fig. 9), the Alto Diamantino basalts form a trend from the OIB field towards the Continental Crust field, suggesting recycle of a continental crust component in the mantle. These features and the different geochemical affinity of the Tristan da Cunha or Gough basalts (Fig. 7) do not support the origin of the Alto Diamantino basalts from a mantle plume. These evidences are in agreement with recent studies on basalts from Brazilian PMP units (De Min et al., 2018; Oliveira et al., 2018; Rocha-Júnior et al., 2013; Rocha-Júnior et al., 2020), on dykes from Southern Espinhaço (Marques et al., 2016) and on Paraguay basalts (Comin-Chiaramonti et al., 2013).

From an isotopic viewpoint, while all the Alto Diamantino basalts fall within the EM-I field (see Stracke, 2012), the slightly more radiogenic Nd isotope ratios of L-Ti compared to H-Ti could be explained adding ca. 7% of a depleted source (DMM; Workman and Hart, 2005) to the EM-I end-member (EM-I component from Armienti and Longo, 2011). The increase of radiogenic Sr isotope ratios at almost constant Nd isotope composition of L-Ti basalts could be instead obtained by adding a small quantity of a 'terrigenous'-related component (i.e. EM-II for ca. 1%; Workman et al., 2004). The involvement of the same isotope end-members to explain the Nd-Sr isotope variability of the Alto Diamantino basalts suggest that the two suites derived from similar mantle sources variably flavoured by metasomatic agents identified as EM-I and EM-II, which originated an heterogeneous mantle column. The two basaltic series have identical La_N/Sm_N ratios (average for both H-Ti and L-Ti is 2.37), but the H-Ti basalts have higher La_N/Yb_N (H-Ti average of 7.21, L-Ti average of 4.52). The differences in REE ratios could be explained i) by melting at different depth, ii) by different degrees of melting of the H-Ti source or iii) by modification due to fractional crystallization. Checking the REE ratios for fractional crystallization effects indicate that La/Sm and La/Yb were not modified for the L-Ti basalts ($m = 0.94$ and 0.99) while they were strongly affected in the H-Ti lavas ($m = 0.49$ and 0.61). Thus, REE ratios cannot constrain the H-Ti

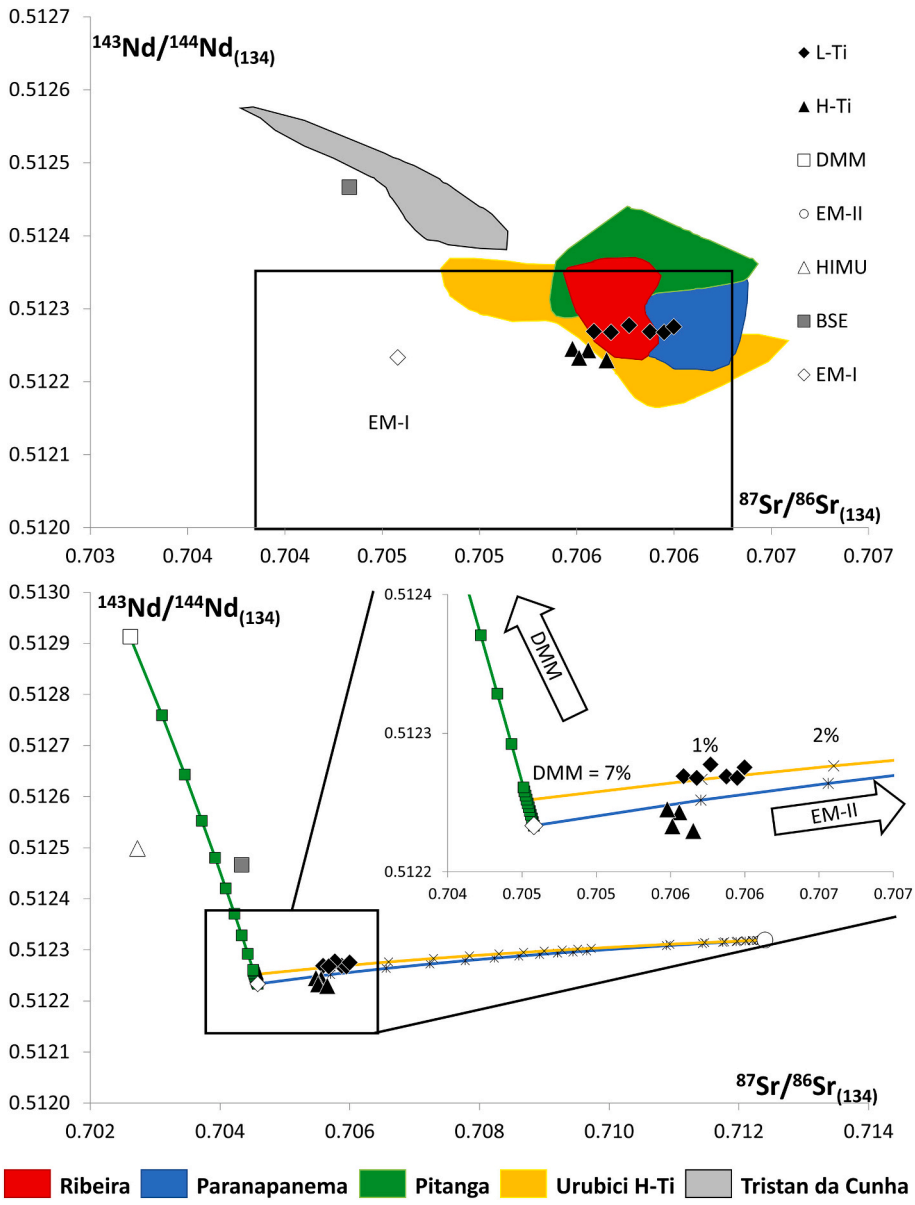

Fig. 8. $^{87}Sr/^{86}Sr$ and $^{143}Nd/^{144}Nd$ variation of Alto Diamantino basalts recalculated at 134 Ma. Fields from PMP basalts are reported for comparison: Pitanga and Paranapanema basalts and Tristan da Cunha are from GEOROC database (http://georoc.mpch-mainz.gwdg.de/georoc/) and Urubici H-Ti basalts are from Peate et al. (1999). DMM is from Workman and Hart (2005), HIMU is from Jackson and Dasgupta (2008), EM-I is from Armienti and Longo (2011) and BSE is from Zindler and Hart (1986).

source. The low La/Yb and Dy/Yb (average 1.85, $m = 1.06$) ratios of L-Ti basalts suggest melting of a lithospheric mantle source, possibly in spinel-facies. This is in agreement with the L-Ti basalt position in the discrimination diagram for large igneous province (LIP) proposed by Pearce et al. (2021) based on Th/Nb vs TiO_2/Yb (Fig. 9). Both L-Ti and H-Ti have Th/Nb ratios not modified by fractional crystallization (m = 1.06 and 1.01 respectively): L-Ti basalts fall in the subduction-modified lithospheric mantle field while H-Ti basalts fall in the OIB field thus suggesting a deeper source (Fig. 9). Lower degree of melting of the source for the H-Ti basalts is instead compatible with their higher trace elements abundances (Figs. 6 and 7). This is also consistent with the genetic model proposed for the Ribeira-type basalts in the northern PMP, which calls upon higher degrees of melting for the L-Ti basalts source (Rocha-Júnior et al., 2020). The relative stratigraphic position of L-Ti basalts on top of H-Ti basalts in Alto Diamantino also supports this interpretation, with initial eruptions of low %F melts (H-Ti) produced during the early stages of PMP activity and successive eruptions of high F melts (L-Ti) produced by a mature PMP activity.

Several studies agree on the main role played by the refertilization of the mantle by hydrous fluids/melts and identified the crustal contaminant in the PMP mantle source either as refertilized phologopite-peridotite (e.g., Marques et al., 1999) or carbonatitic components (De Min et al., 2018; Marques et al., 2016) or eclogite-derived melts (e.g., Rocha-Júnior et al., 2020). The positive Ba anomaly of the Alto Diamantino basalts and their high Rb abundance might indicate the occurrence of a hydrated mineral phase in the mantle source derived from crystallization of hydrous fluids/melts during a refertilization event. The main hydrous minerals within the mantle are amphibole and phlogopite. Phlogopite is the main carrier of Ba, Pb and K (Rosenbaum, 1993) but Alto Diamantino basalts show lower K content compared to Na (Fig. 5) and Pb is not enriched but sometimes depleted (Figs. 6 and 7). The K/Rb ratio of H-Ti basalts shows absence of modification from fractional crystallization ($m = 0.93$). Accordingly, the H-Ti basalts fall in the amphibole-disseminated field of the K/Rb vs K classification diagram of Ionov et al. (1997) supporting the hypothesis of modal metasomatism in the source (Fig. 9). The H-Ti suite shows higher alkali content compared to the L-Ti (Fig. 5) and a more enriched Nd-Sr isotopic composition (Fig. 8). These differences suggest that the L-Ti basalts crystallized from a melt produced by a mantle source similar to the one of the H-Ti, but where the crustal component was more diluted.

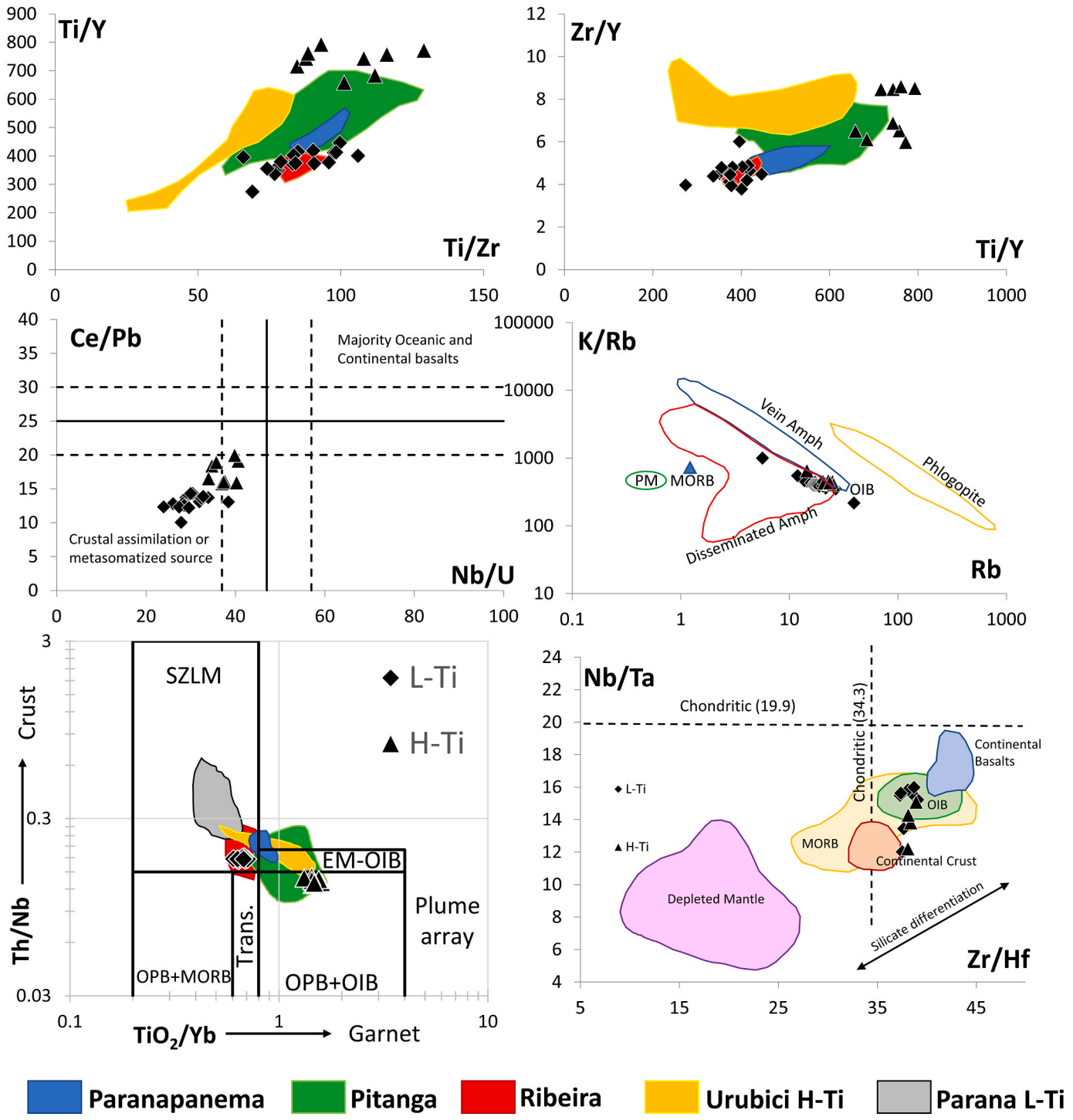

Fig. 9. Ti/Y vs Ti/Zr and Zr/Y vs Ti/Y diagrams. Ce/Pb vs Nb/U diagram from Hofmann et al. (1986). K/Rb vs K diagram from Ionov et al. (1997). Nb/Ta vs Zr/Hf diagram from Pfänder et al. (2007). TiO_2/Yb vs. Th/Nb discriminant diagram after Pearce et al. (2021). For comparison, basalts from the alkaline Mesozoic magmatism of the PMP are reported: Pitanga, Paranapanema, Ribeira and L-Ti basalts (GEOROC database (http://georoc.mpch-mainz.gwdg.de/georoc/) and Urubici H-Ti basalts (Peate et al., 1999). Acronyms are from Pearce et al. (2021): Ocean Plateau Basalt (OPB); Mid-Ocean Ridge Basalt (MORB); Ocean Island Basalt (OIB); Subduction-modified Lithospheric Mantle (SZLM).

Recently, based on Os isotopes and geophysical investigations, the mantle source of Ribeira basalts was attributed to shards of old Archean sub-lithospheric mantle, different from the younger mantle sequence responsible for the genesis of H-Ti and others L-Ti suites (Rocha-Júnior et al., 2020). The geochemical similarity of the Alto Diamantino L-Ti basalts with the Ribeira basalts suggests that the metasomatic event affecting the two suites could be the same. These ages indicate that the refertilization of the sub-continental lithospheric mantle might have taken place during the formation of the Gondwana supercontinent during the Neoproterozoic-Cambrian periods, when several suture zones surrounding the Paraná basin and subduction processes were active (Rocha-Júnior et al., 2020).

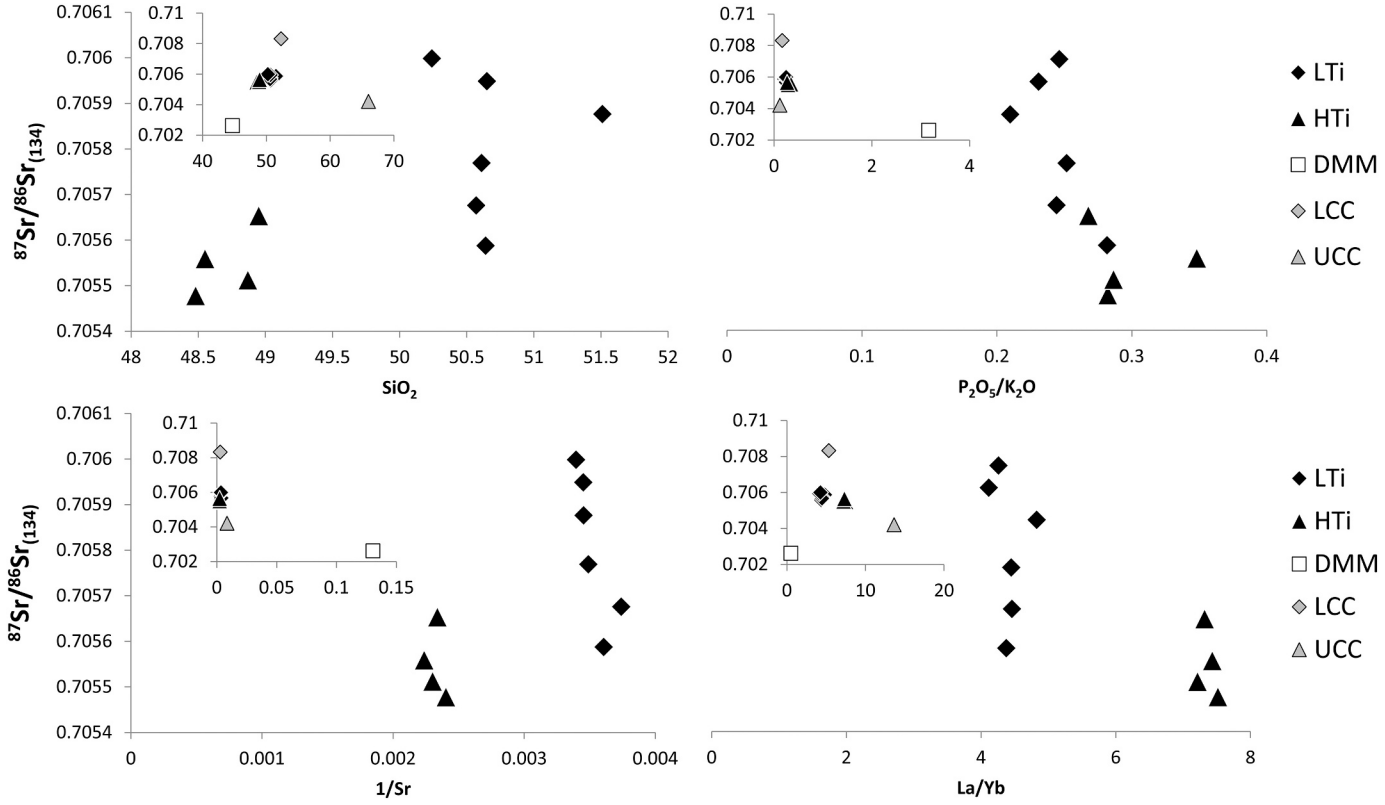

Fig. 10. $^{87}Sr/^{86}Sr_{134}$ vs SiO_2, P_2O_5/K_2O, 1/Sr and La/Yb diagrams.

7. Conclusions

A number of observations and conclusions can be drawn from our geochronological and geochemical investigation of the Alto Diamantino basalts:

1) the Alto Diamantino basalts are genetically related to the Parana-Etendeka Magmatic Province, thus representing its most north-western occurrence at the border with the Paraná Basin.
2) the major element composition of these basalts defines two distinct groups, a low-Ti group ($TiO_2 < 3$ wt%) and a high-Ti ($TiO_2 > 3$ wt%) group, broadly coeval (133.2 ± 0.8 Ma and 134.7 ± 1.0 Ma respectively) totally similar to previously recognized groups of PMP basalts.
3) the field distribution of the basalts in the Alto Diamantino region suggests that L-Ti (Ribeira-type) basalts are stratigraphically above the H-Ti (Pitanga-type) ones. This implies that the production of high and low Ti suites in the PMP is not a time-dependent process.
4) the absence of crustal assimilation and the different geochemical and isotopic affinity of the Alto Diamantino basalts compared to the Tristan da Cunha mantle plume lavas suggest that they originated from a metasomatized subcontinental lithospheric mantle. Higher Na than K in Alto Diamantino basalts, K/Rb ratios and absence of Pb enrichments point to the occurrence of amphibole in the mantle source.
5) the different Th/Nb and TiO_2/Yb ratios suggest crystallization of the H-Ti basalts from melts derived by lower mantle degree of melting from a source deeper than the one producing the L-Ti basalts melts.

Declaration of Competing Interest

The authors declare that they have no known competing financial interests or personal relationships that could have appeared to influence the work reported in this paper.

Acknowledgements

We acknowledge financial support from the Programmi di Ricerca di Interesse Nazionale of the Italian Ministero dell'Istruzione, dell'Università e della Ricerca (protocol PRIN20178LPCPW), Conselho Nacional de Pesquisas (CNPq), Brazil, and FAGEO–UFMT, (Faculdade de Geociéncias - Universidade Federal de Mato Grosso, Brazil).

Appendix A. Ar-Ar data

Supplementary data to this article can be found online at https://doi.org/10.1016/j.lithos.2022.106797.

References

Armienti, P., Longo, P., 2011. Three-dimensional representation of geochemical data from a multidimensional compositional space. Int. J. Geosci. 2, 231–239.
Arndt, N.T., Czamanske, G.K., Wooden, J.L., Federenko, V.A., 1993. Mantle and crustal contributions to continental flood volcanism. Tectonophysics 223, 39–52.
Barros, A.M., Da Silva, R.H., Cardoso, O.R.F.A., Freire, F.A., De Souza Jr., J.J., Rivetti, M., Da Luz, O.S., De Palmeira, R.C.D.B., Tassinari, C.G.C., 1982. Folha Cuiabá, SD-21, Projeto RadamBrasil, Ministério das Minas e Energia, Rio de Janeiro, 26 (540 p).
Bellieni, G., Comin-Chiaramonti, P., Marques, L.S., Melfi, A.J., Nardy, A.J.R., Piccirilo, E. M., Roisenberg, A., 1984. High- and low-TiO2 flood basalts from the Paraná plateau (Brazil): petrology and geochemical aspects bearing on their mantle origin. Neues Jahrbuch für Mineralogie 150, 273–306.
Piccirillo, E.M., Civetta, L., Petrini, R., Longinelli, A., Comin-Chiaramonti, P., Marques, L. S., Melfi, A.J., 1989. Regional variations within the Paraná flood basalts (southern Brazil): evidence for subcontinental mantle heterogeneity and crustal contamination. Chem. Geol. 75, 103–122.
Comin-Chiaramonti, P., De Min, A., Girardi, V.A.V., Ruberti, E., 2011. Post-Paleozoic magmatism in Angola and Namibia: A review. In: Beccaluva, L., Bianchini, G., Wilson, M. (Eds.), Volcanism and Evolution of the African Lithosphere, Geological Society of America, Special Paper, vol. 478, pp. 223–247.
Comin-Chiaramonti, P., De Min, A., Cundari, A., Girardi, V.A.V., Ernesto, M., Gomes, C. B., Riccomini, C., 2013. Magmatism in the Asunción-Sapucai-Villarrica graben (Eastern Paraguay) revisited. Petrological, geophysical, geochemical and geodynamic inferences. J. Geol. Res. 2013, 1–22. https://doi.org/10.1155/2013/590835 (ID 590835).

Cordani, U.G., Teixeira, W., D'Agrella-Filho, M.S., Trindade, R.I., 2009. The position of the Amazonian Craton in supercontinents. Gondwana Res. 15 (396–40).
Correia, C.T., Girardi, V.A.V., Kirk, J.D., Nardy, A.J.R., Petronilho, L.A., Tasssinari, C.G. C., 2011. Re-Os pattern of high-Ti Paraná flood basalts, Brazil: preliminary inferences on their mantle sources. In: XII Congresso Brasileiro de Geoquímica e III Simpósio de geoquímica dos Paises do Mercosul, 2011, Gramados. Anais, 2011. v. CD Rom, pp. 1143–1146.
De Min, A., Callegaro, S., Marzoli, A., Nardy, A.J., Chiaradia, M., Marques, L.S., Gabbarrini, I., 2018. Insights into the petrogenesis of low- and high-Ti basalts: Stratigraphy and geochemistry of four lava sequences from the Central Paraná basin. J. Volcanol. Geotherm. Res. 355, 232–252.
Eiler, J.M., Farley, K.A., Valley, J.W., Stolper, E.M., Hauri, E.H., Craig, H., 1995. Oxygen isotope evidence against bulk recycled sediment in the mantle sources of Pitcairn Island lavas. Nature 377, 138–141.
Eisele, J., Sharma, M., Galer, S.J.G., Blichert-Toft, J., Devey, C.W., Hofmann, A.W., 2002. The role of sediment recycling in EM-1 inferred from Os, Pb, Hf, Nd, Sr isotope and trace element systematics of the Pitcairn hotspot. Earth Planet. Sci. Lett. 196, 197–212.
Ellam, R.M., Cox, K.G., 1991. An interpretation of Karoo picrite basalts in terms of interaction between asthenospheric magmas and mantle lithosphere. Earth Planet. Sci. Lett. 105, 330–342.
Ernesto, M., Marques, L.S., Piccirillo, E.M., Molina, E.C., Ussami, N., Comin-Chiaramonti, P., Bellieni, G., 2002. Paraná Magmatic Province-Tristan da Cunha plume system: fixed versus mobile plume, petrogenetic considerations and alternative heat sources. J. Volcanol. Geotherm. Res. 118, 15–36.
Ewart, A., Milner, S.C., Armstrong, R.A., Duncan, A.R., 1998. Etendeka volcanism of the Goboboseb Mountains and Messum Igneous complex, Namibia. Part I: geochemical evidence of early cretaceous Tristan plume melts and the role of crustal contamination in the Paraná-Etendeka CFB. J. Petrol. 39 (2), 191–225.
Ewart, A., Marsh, J.S., Milner, S.C., Duncan, A.R., Kamber, B.S., Armstrong, R.A., 2004. Petrology and geochemistry of early cretaceous bimodal continental flood volcanism of the NW Etendeka, Namibia. Part 1: introduction, mafic lavas and re-evaluation of mantle source components. J. Petrol. 45, 59–105.
Fodor, R.V., 1987. Low- and high-TiO2 flood basalts of southern Brazil: origin from a picritic parentage and a common mantle source. Earth Planet. Sci. Lett. 84, 423–430.
Frey, F.A., Weis, D., Borisova, Y.A., Xu, G., 2002. Involvement of continental crust in the formation of the cretaceous Kerguelen plateau: new perspectives from ODP Leg 120 Sites. J. Petrol. 43, 1207–1239.
Gibson, S.A., Thompson, R.N., Day, J.A., Humphris, S.E., Dickin, A.P., 2005. Melt generation processes associated with the Tristan mantle plume: constraints on the origin of EM-I. Earth Planet. Sci. Lett. 237, 744–767.
Giovanardi, T., Girardi, V.A.V., Teixeira, W., Mazzucchelli, M., 2019. Mafic dyke swarms at 1882, 535 and 200 Ma in the Carajás region, Amazonian Craton: SreNd isotopy, trace element geochemistry and inferences on their origin and geological settings. J. S. Am. Earth Sci. 92, 197–208.
Gomes, A.S., Vasconcelos, P.M., 2021. Geochronology of the Paraná-Etendeka large igneous province. Earth Sci. Rev. 220, 103716 https://doi.org/10.1016/j.earscirev.2021.103716.
Hawkesworth, C.J., Mantovani, M.S.M., Taylor, P.N., Palacz, Z., 1986. Evidence from the Parana of South Brazil for a continental contribution to Dupal basalts. Nature 322, 356–359.
Hacker, B.R., Kelemen, P.B., Behn, M.D., 2015. Continental Lower Crust. Annu. Rev. Earth Planet. Sci. 43, 167–205.
Hawkesworth, C.J., Mantovani, M.S.M., Peate, D.W., 1988. Lithosphere remobilization during Paraná magmatism. J. Petrol. Spec. Lithosphere Issue 205–233.
Hoernle, K., Rohde, J., Hauff, F., Garbe-Schönberg, D., Homrighausen, S., Werner, R., Morgan, J.P., 2015. How and when plume zonation appeared during the 132Myr evolution of the Tristan Hotspot. Nat. Commun. 6, 7799.
Hofmann, A.W., 1988. Chemical differentiation of the Earth: the relationship between mantle, continental crust and oceanic crust. Earth Planet. Sci. Lett. 90, 297–314.
Hofmann, A.W., Jochum, K.P., Seufert, M., White, W.M., 1986. Nb and Pb in oceanic basalts: new constraints on mantle evolution. Earth Planet. Sci. Lett. 79, 33–45.
Ionov, D.A., Griffin, W.L., O'Reilly, S.Y., 1997. Volatile-bearing minerals and lithophile trace elements in the upper mantle. Chem. Geol. 141, 153–184.
Jackson, M.G., Dasgupta, R., 2008. Compositions of HIMU, EM1, and EM2 from global trends between radiogenic isotopes and major elements in ocean island basalts. Earth Planet. Sci. Lett. 276, 175–186.
Janasi, V.A., Freitas, V.A., Heaman, L.H., 2011. The onset of flood basalt volcanism, Northern Paraná Basin, Brazil: a precise U-Pb baddeleyite/zircon age for a Chapecó-type dacite. Earth Planet. Sci. Lett. 302, 147–153.
Kempton, P.D., Pearce, J.A., Barry, T.L., Fitton, J.G., Langmuir, C.H., Christie, D.M., 2002. Sr–Nd–Pb–Hf isotope results from ODP Leg 187: evidence for mantle dynamics of the Australian-Antarctic Discordance and origin of the Indian MORB source. Geochem. Geophys. Geosyst. 3 (10.29/2002GC000320).
Klein, E.M., 2004. Geochemistry of the igneous oceanic crust. In: Holland, H.D., Turekian, K.K. (Eds.), Treatise on Geochemistry, vol. 3. Elsevier, Amsterdam, pp. 433–463.
Kuiper, K.F., Deino, A., Hilgen, F.J., Krijgsman, W., Renne, P.R., Wijbrans, J.B., 2008. Synchronizing Rock Clocks of Earth History: Science, 320, pp. 500–504.
Lacerda Filho, J.V., Abreu Filho, W., Valente, R.C., Oliveira, C.C., Albuquerque, M.C., 2004. Geologia e Recursos Minerais do Estado de Mato Grosso, Programa de Geologia do Brasil, Companhia Pesquisa Recursos Minerais, Cuiabá (220p).
Le Bas, M.J., Le Maitre, R.W., Woolley, A.R., 1992. The construction of the total alkali-silica chemical classification of volcanic rocks. Mineral. Petrol. 46, 1–22.
Lee, J.Y., Marti, K., Severinghaus, J.P., Kawamura, K., Yoo, H.S., Lee, J.B., Kim, J.S., 2006. A redetermination of the isotopic abundances of atmospheric Ar. Geochim. Cosmochim. Acta 70, 4507–4512.
Luchetti, A.C.F., Nardy, A.J.R., Madeira, J., 2018. Silicic, high- to extremely high-grade ignimbrites and associated deposits from the Paraná Magmatic Province, southern Brazil. J. Volcanol. Geotherm. Res. 355, 270–286.
Lyubetskaya, T., Korenaga, J., 2007. Chemical composition of Earth's primitive mantle and its variance: 1. Method and results. J. Geophys. Res. 112, B03211.
Machado, F.B., Rocha-Júnior, E.R.V., Marques, L.S., Nardy, A.J.R., 2015. Volcanological aspects of the northwest region of Paraná continental flood basalts (Brazil). Solid Earth 6, 227–241.
Machado, F.B., Rocha-Júnior, E.R.V., Marques, L.S., Nardy, A.J.R., Zezzo, L.V., Marteleto, N.S., 2018. Geochemistry of the Northern Paraná Continental Flood Basalt (PCFB) Province: implications for regional chemostratigraphy. Braz. J. Geol. 48 (2), 177–199.
Marques, L.S., Dupré, B., Piccirillo, E.M., 1999. Mantle source compositions of the Paraná Magmatic Province: evidence from trace element and Sr-Nd-Pb isotope geochemistry. J. Geodyn. 28, 439–459.
Marques, L.S., Rocha-Junior, E.R.V., Babinski, M., Carvas, K.Z., Petronilho, L.A., De Min, A., 2016. Lead isotope constraints on the mantle sources involved in the genesis of Mesozoic high-Ti tholeiite dykes (Urubici type) from the São Francisco Craton (Southern Espinhaço, Brazil). Braz. J. Geol. 46, 105–122.
McDonough, W.F., Sun, S.S., 1995. The composition of the Earth. Chem. Geol. 120, 223–253.
Mohlzahn, M., Reisberg, L., Worner, G., 1996. Os, Sr, Nd, Pb, O.isotope and trace element data from the Ferrar flood basalts, Antartica: evidence for an enriched subcontinental lithospheric source. Earth Planet. Sci. Lett. 144, 529–546.
Mori, P.E., Reeves, S., Correia, C.T., Haukka, M., 1999. Development of a Fused Glass Disc XRF Facility and Comparison with the Pressed Powder Pellet Technique at Instituto de Geociências, University of São Paulo: Revista Brasileira de Geociências, 29, pp. 441–446.
Navarro, M.S., Andrade, S., Ulbrich, H.H.G.J., Gomes, C.B., Girardi, V.A.V., 2008. The analysis of rare earth elements with ICP-MS in basaltic and related rocks: Testing the efficiency of sample decomposition procedures. Geostand. Geoanal. Res. 32 (2), 167–180.
Nebel, O., Scherer, E.E., Mezger, K., 2011. Evaluation of the ^{87}Rb decay constant by age comparison against the U-Pb system. Earth Planet. Sci. Lett. 301, 1–8.
Oliveira, A.L., Pimentel, M.M., Fuck, R.A., Oliveira, D.C., 2018. Petrology of Jurassic and cretaceous basaltic formations from the Parnaíba Basin, NE Brazil: correlations and associations with large igneous provinces. In: Daly, M.C., Fuck, R.A., Julià, J., MacDonald, D.I.M., Watts, A.B. (Eds.), Cratonic Basin Formation: A Case Study of the Parnaíba Basin of Brazil.
Pearce, J.A., Ernst, R.E., Peate, D.W., Rogers, C., 2021. LIP printing: use of immobile element proxies to characterize large Igneous Provinces in the geologic record. Lithos 392–393, 106068.
Peate, D., 1997. The Parana-Etendeka Province. In: Mahoney, J.J., Coffin, M.F. (Eds.), Large Igneous Provinces: Continental, Oceanic, and Planetary Flood Volcanism, American. Geophysical. Union Geophysical Monogr, vol. 100, pp. 217–246.
Peate, D.W., Hawkesworth, C.J., Mantovani, M.S.M., Shukovsky, W., 1990. Mantle plumes and flood basalt stratigraphy in the Paraná, South America. Geology 18, 1223–1226.
Peate, D.W., Hawkesworth, C.J., Mantovani, M.S.M., 1992. Chemical stratigraphy of the Paraná lavas (South America): classification of magma types and their spatial distribution. Bull. Volcanol. 55, 119–139.
Peate, D.W., Hawkesworth, C.J., Mantovani, M.S.M., Rogers, N.W., Turner, S.P., 1999. Petrogenesis and stratigraphy of the high-Ti/Y Urubici magma type in the Paraná flood basalt province and implications for the nature of 'Dupal'- type mantle in the South Atlantic region. J. Petrol. 40 (3), 451–473.
Petrini, R., Civetta, L., Piccirillo, E.M., Bellieni, G., Comin-Chiaramonti, P., Marques, L.S., Melfi, A.J., 1987. Mantle heterogeneity and crustal contamination in the genesis of low-Ti continental flood basalts from the Paraná plateau (Brazil): Sr-Nd isotope and geochemical evidence. J. Petrol. 28, 701–726.
Pfänder, J.A., Münker, C., Stracke, A., Mezger, K., 2007. Nb/Ta and Zr/Hf in ocean island basalts — Implications for crust–mantle differentiation and the fate of Niobium. Earth Planet. Sci. Lett. 254, 158–172.
Piccirillo, E.M., Melfi, A.J., 1988. The Mesozoic Flood Volcanism of the Paraná Basin: Petrogenetic and Geophysical Aspects. Universidade de São Paulo, São Paulo, p. 600.
Plank, T., Langmuir, C.H., 1998. The chemical composition of subducting sediment and its consequences for the crust and mantle. Chem. Geol. 145, 325–394.
Reis, N.J., Teixeira, W., D'Agrella-Filho, M.S., Bettencourt, J.S., Ernst, R.E., Goulart, L.E., 2021. Large Igneous Provinces of the Amazonian Craton and their metallogenic potential in proterozoic times. Geol. Soc. Lond., Spec. Publ. 518 https://doi.org/10.1144/SP518-2021-7.
Renne, P.R., Ernesto, M., Pacca, I.G., Coe, R.S., Glen, J., Prev, M., Perrin, M., 1992. The age of Parana flood volcanism, rifting of Gondwanaland, and the Jurassic - cretaceous boundary. Science 258, 975–979.
Renne, P.R., Balco, G., Ludwig, K.R., Mundil, R., Min, K., 2011. Response to the comment by W.H. Schwarz et al. on "Joint determination of 40K decay constants and 40Ar*/40K for the fish Canyon sanidine standard, and improved accuracy for 40Ar/39Ar geochronology" by P.R. Renne et al. (2010). Geochim. Cosmochim. Acta 75, 5097–5100.
Rocha-Campos, A.C., Cordani, U.G., Kawashita, K., Sonoki, H.M., Sonoki, I.K., 1988. Age of Paraná flood volcanism. In: Piccirillo, E.M., Melfi, A.J. (Eds.), The Mesozoic Flood Volcanism of the Paraná Basin, Petrogenetic and Geophysical Aspects. University of São Paulo, Brazil, pp. 24–45.

Rocha-Júnior, E.R.V., Puchtel, I.S., Marques, L.S., Walker, R.J., Machado, F.B., Nardy, A. J.R., Babinski, M., Figueiredo, A.M.G., 2012. Re-Os isotope and highly siderophile element systematics of the Paraná Continental Flood Basalts (Brazil). Earth Planet. Sci. Lett. 337-338, 164–173.

Rocha-Júnior, E.R.V., Marques, L.S., Babinski, M., Nardy, J.R.A., Figueiredo, A.M.G., Machado, Fábio B., 2013. Sr-Nd-Pb isotopic constraints on the nature of the mantle sources involved in the genesis of the high-Ti tholeiites from northern Paraná. Continental Flood Basalts (Brazil). J. S. Am. Earth Sci. 46, 9–25.

Rocha-Júnior, E.R.V., Marques, L.S., Babinski, M., Machado, F.B., Petronilho, L.A., Nardy, J.R.A., 2020. A telltale signature of Archean lithospheric mantle in the Paraná continental flood basalts genesis. Lithos 364–365, 105519.

Roden, M.F., Trull, T., Hart, S.R., Frey, F.A., 1994. New He, Nd, Pb, and Sr isotopic constraints on the constitution of the Hawaiian plume: results from Koolau Volcano, Oahu, Hawaii, USA. Geochim. Cosmochim. Acta 58, 1431–1440.

Rosenbaum, J.M., 1993. Mantle phlogopite: a significant lead repository? Chem. Geol. 106 (3–4), 475–483.

Roverato, M., Giordano, D., Giovanardi, T., Juliani, C., Polo, L., 2019. The 2.0–1.88 Ga Paleoproterozoic evolution of the southern Amazonian Craton (Brazil): an interpretation inferred by lithofaciological, geochemical and geochronological data. Gondwana Res. 70, 1–24.

Rudnick, R.L., The CrustH.D. Holland, 2003. Composition of the continental crust. In: Rudnick, R.L., Gao, S., Turekian, K.K. (Eds.), Treatise on Geochemistry, vol. 3. Elsevier-Pergamon, Oxford, pp. 1–64, 2003.

Sarmento, C.C.T., Sommer, C.A., Lima, E.F., 2017. Mafic subvolcanic intrusions and their petrologic relation with the volcanism in the south hinge Torres Syncline, Paraná-Etendeka Igneous Province, southern Brazil. J. S. Am. Earth Sci. 77, 70–91.

Sato, K., Tassinari, C.C.G., Kawashita, K., Petronilho, L., 1995. O Método geocronológico Sm–Nd no IG/USP e suas aplicações. An. Acad. Bras. Cienc. 67, 313–336.

Steiger, R.H., Jäger, E., 1977. Subcommission on geochronology: Convention on the use of decay constants in geo- and cosmochemistry. Earth Planet. Sci. Lett. 36, 359–362.

Stracke, A., 2012. Earth's heterogeneous mantle: a product of convection-driven interaction between crust and mantle. Chem. Geol. 330–331, 274–299.

Sun, S.-S., McDonough, W.F., 1989. Chemical and isotopc systematics of oceanic basalts: Implications for mantle composition and processes. In: Saunders, A.D., Norry, M.J. (Eds.), Magmatism in the Ocean Basins. Geological Society, London, pp. 313–334.

Teixeira, W., Hamilton, M.A., Lima, G.A., Matos, R., Ernst, R.E., 2015. Precise ID-TIMS U-Pb baddeleyite ages (1110-1112 Ma) for the Rincón del Tigre-Huanchaca large igneous province (LIP) of the Amazonian Craton: Implications for the Rodinia supercontinent. Precambrian Res. 265, 273–285.

Teixeira, W., Reis, N.J., Bettencourt, J.S., Klein, E.F., Oliveira, D., 2019. Intraplate Proterozoic magmatism in the Amazonian Craton reviewed: geochronology, crustal tectonics and global barcode matches. In: Rajesh et al. "Dyke Swarms of the World-A modern perspective". Springer Geology, pp. 111–154. https://doi.org/10.1007/978-981-13-1666-1_4.

Thiede, D.S., Vasconcelos, P.M., 2010. Paraná flood basalts: rapid extrusion hypothesis confirmed by new 40Ar/39Ar results. Geology 38 (8), 747–750.

Vasconcelos, P.M., Onoe, A.T., Kawashita, K., Soares, A.J., Teixeira, W., 2002. 40Ar/39Ar geochronology at the Instituto de Geociências, USP: instrumentation, analytical procedures, and calibration. Ann. Braz. Acad. Sci. 74, 297–342.

Willbold, M., Stracke, A., 2006. The trace element composition of mantle end-members: implications for recycling of oceanic and upper/lower continental crust. Geochem. Geophys. Geosyst. 7, Q04004. https://doi.org/10.1029/2005GC001005.

Woodhead, J.D., Greenwood, P., Harmon, R.S., Stoffers, P., 1993. Oxygen isotope evidence for recycled crust in the source of EM-type Ocean island basalts. Nature 362, 809–813.

Workman, R.K., Hart, S.R., 2005. Major and trace element composition of the depleted MORB mantle (DMM). Earth Planet. Sci. Lett. 231, 53–72.

Workman, R.K., Hart, S.R., Jackson, M., Regelous, M., Farley, K.A., Blusztajn, J., Kurz, M., Staudigel, H., 2004. Recycled metasomatized lithosphere as the origin of the enriched mantle II (EM2) endmember: evidence from the Samoan Volcanic chain. Geochem. Geophys. Geosyst. 5 (4), Q04008.

Zindler, A., Hart, S.R., 1986. Chemical geodynamics. Annu. Rev. Earth Planet. Sci. 14, 493–571.